Energy and Built Environment xxx (xxxx) xxx

Contents lists available at ScienceDirect

Energy and Built Environment

journal homepage: http://www.keaipublishing.com/en/journals/energy-and-built-environment/

Full Length Article

Characterization, optimization, and performance evaluation of PCM with Al_2O_3 and ZnO hybrid nanoparticles for photovoltaic thermal energy storage

Md. Golam Kibria[a,*], Utpol K. Paul[a], Md. Shahriar Mohtasim[a], Barun K. Das[a,b], N.N. Mustafi[a]

[a] Department of Mechanical Engineering, Rajshahi University of Engineering & Technology, Rajshahi-6204, Bangladesh
[b] School of Engineering, Edith Cowan University, Joondalup, WA-6027, Australia

ARTICLE INFO

Keywords:
Photovoltaic
Phase change materials
Nano-materials
Response surface methodology
Optimization

ABSTRACT

The electrical efficiency of the photovoltaic (PV) panel is affected significantly with increased cell temperature. Among various approaches, the use of Phase Change Materials (PCMs) with nanoparticles is currently one of the most effective for reducing and managing the temperature of PV panels. In this study, paraffin wax as PCM with different loading levels (0.5 %, 1 %, and 2 %) of hybrid nanoparticles Al_2O_3 and ZnO were successfully synthesized and their effects on the performance of the Photovoltaic-Thermal (PVT) system were investigated experimentally. Additionally, a prediction model was developed to analyze the interaction between the operating factors (independent variable) and response factors (dependent variable) of the PVT/PCM and PVT with Hybrid nano-PCM (PVT/HNPCM) systems based on response surface methodology (RSM). Experimental results showed that compared to only PCM, the thermal conductivity of HNPCM increased by 24.68 %, 28.57 %, and 41.56 % for the inclusion of 0.5 %, 1 %, and 2 % hybrid nanomaterial respectively. The electrical efficiency of the PVT/HNPCM, and PVT/PCM system enhanced by 31.46 % and 28.70 % respectively compared to the conventional PV system in this study. With a cooling-water mass flow rate of 0.0021 kg/s, the highest thermal efficiency of 47 % was achieved for the PVT/PCM system, whereas 51.28 % was achieved for the PVT/HNPCM system. The analysis of the variance test yielded a P value <0.0001 which is less than 0.05 for the model of overall efficiency for PVT/PCM and PVT/HNPCM system, indicating the suggested model's appropriateness and statistical significance. These optimal conditions are observed when the solar intensity ranges from 774 W/m^2 to 809 W/m^2 and the mass flow rate is 0.002 kg/s for both the PVT/PCM and PVT/HNPCM systems. However, these systems advance sustainable urban development and climate goals by combining PV panels' electrical generation with thermal energy harvesting, boosting overall energy efficiency in the built environment.

1. Introduction

Energy is intertwined with all elements of economic, social, environmental, and the development of the standard of living. With the world population reaching 79 billion, the demand for energy is rising quickly and is barely being met [1]. This increasing demand for energy leads to the dependency on fossil fuels resulting in the rapid depletion of fuels and emitting of greenhouse gas into the environment. Hence, the entire world is moving fast toward renewable sources of energy to mitigate all the challenges [2-4]. In times of energy crisis, renewable energy sources can be extremely important due to their abundance, low cost, and low levels of greenhouse gas emission. Shifting to renewable sources of energy is mandatory for energy diversification and for alleviating climate change [5,6]. Solar energy can be regarded as a clean, domestic, and inexhaustible source of renewable energy with no adverse impact on the environment [7,8]. The sun is capable of releasing a significant quantity of energy as electromagnetic radiation [9]. With the use of solar technology, this electromagnetic radiation can be transformed into heat [10] and electrical energy [11]. However, solar energy can't be harnessed directly into a useful form of energy without solar technology. The solar technology includes photovoltaic panels, solar still, and solar collector technology [12]. Solar photovoltaic thermal (PVT) systems have the potential to generate both electric and thermal energy, boosting system's overall performance than the PV panels alone [13]. Only 10 to 23 % of incoming irradiance is converted by PV panels into electricity due to their low efficiency; the remaining energy is discharged as heat energy [14]. PV panel efficiency reduces with the increase in cell temperature [15-17], therefore, thermal management of PV systems is required to improve electrical conversion efficiency. It has been explored from the published literature that for every 1 °C increase in cell

* Corresponding author at: Department of Mechanical Engineering, Rajshahi University of Engineering & Technology, Rajshahi-6204, Bangladesh.
E-mail address: kibria@me.ruet.ac.bd (Md.G. Kibria).

https://doi.org/10.1016/j.enbenv.2024.06.001
Received 30 December 2023; Received in revised form 3 June 2024; Accepted 4 June 2024
Available online xxx

Nomenclature

Al_2O_3	Aluminum oxide
ZnO	Zinc Oxide
V_{max}	Maximum voltage
I_{max}	Maximum current
V_{oc}	Open circuit voltage (V)
I_{sc}	Short circuit current (A)
FF	Fill factor
E_{el}	Electrical power (W)
E_{th}	Thermal power (W)
E_{sun}	Sun energy
G	Solar irradiation (W)
A_c	Area of solar panel (m^2)
m_f	Mass flow rate of the coolant
$C_{p,f}$	Specific heat of the fluid
$\ddot{G}$	Rate of solar irradiation (W/m^2)
$T_{f,in}$	Inlet temperature of the fluid (°C)
$T_{f,out}$	Outlet temperature of the fluid (°C)
T_{amb}	Ambient temperature (°C)
T_{sun}	Sun temperature (°C)
df	Degree of freedom

Abbreviation

PV	Photovoltaic
PCM	Phase Change Material
PW	Paraffin wax
PVT/HNPCM	Photovoltaic thermal/hybrid nano-PCM
PVT	Photovoltaic thermal
HNPCM	Hybrid nano-PCM
NPCM	Nano-PCM
GNP	Graphene nanoplatelet
MWCNT	Multi-walled carbon nano-tube
NP	Nanoparticle
FTIR	Fourier transfer infrared spectroscopy
SEM	Scanning electron microscope
TGA	Thermogravimetry analysis
RSM	Response surface methodology
DSC	Differential scanning calorimetric
CCD	Central composite design
ANOVA	Analysis of variance
PEG	Polyethylene glycol

Symbols

τ_g	Glass transmissivity
α_{cell}	Cell absorptivity
η_{ov}	Overall electrical efficiency (%)
η_{el}	Electrical efficiency (%)
η_{th}	Thermal efficiency (%)

temperature, there is a 0.35 percent drop in PV output power [18]. In this context, several strategies have been employed to enhance the PVT module power output including nano coolant [19,20], heat pipe cooling [21], thermoelectric cooling [22], utilization of phase change materials (PCM) [23,24], and nanoparticles integrated PCM [25,26]. The benefits of PCM utilization include the elimination of the need for auxiliary energy consumption, which is required by some active cooling systems [27]. Additionally, PCMs are non-toxic, non-corrosive, chemically stable, and have a high latent heat of fusion [28]. Furthermore, their melting point is rather near to the PV module operational temperature [27,29]. The passive cooling of PV module with PCM could reduce the cell temperature of 6.1 °C, subsequently improving the efficiency of 5.3 % [30].

Thermal collector is installed rear the PV panel to convert the unwanted heat generated in PV modules into useful energy for the improvement of the PVT system overall performance. Several studies have focused on using PCM for passive cooling of PV modules as active cooling such as water and air cooling require auxiliary power. Gürbüz et al. [31] obtained 30.56 W of electrical power and 1.21 W of thermal energy stored in PCM while experimentally investigating a PVT system with RT55 as PCM and water as cooling media. Lauric acid was utilized as PCM by Hossain et al. [32] in tiny aluminum foil packets that were positioned around a PVT/PCM system's flow channel. The PVT/PCM system's maximum thermal efficiency was figured out to be 87.72 %, whereas it was discovered that PV and PVT/PCM systems had the maximum electrical efficiency at 9.88 % and 11.08 %, respectively in this study. Rezvanpour et al. [33] looked into the impact of calcium chloride hexahydrate as PCM on PV module performance using both numerical and experimental methods. They achieved a cell temperature reduction of 26.3 °C, while about 24.68 % increment in the electric power of the PV/PCM system. Water-based PVT systems with and without PCM efficacy was examined by Preet et al. [34]. When compared to PV and PVT systems, they discovered that the temperature of PVT/PCM decreased by 53 % and 47 %, respectively, at a mass flow rate of 0.031 kg/s of water. The highest enhancement in electrical efficiency of PVT/PCM reached 12.6 %, while the PVT system was 10.66 % than the conventional PV with the same water flow rate. Regardless of better thermal properties and performance intensification of PVT collector, there are few drawbacks with PCMs such as, some PCMs have rusted the PCM container, and it becomes toxic and facing disposal problem [35]. Furthermore, some PCMs might not properly release stored heat energy because they lack heat exchanger designs. Therefore, it cannot fully meet the next day's maximum storing capacity. Regarding PCM and HNPCM-based PVT systems, despite being a very cutting-edge technology, they have significant drawbacks, such as a lack of standard for synthesis of HNPCM and inconsistent measurement approaches for different factors to measure the behavior of HNPCM [36]. One major problem that increases the expense of operations and maintenance and decreases the end user's appeal of this technology is the constraints of repeatedly using nano-PCM and how hard it is to replace them. Some nano particles have issues with dispersion in PCM and fluids. A small number of nano PCMs also experience settling issues after a few operational cycles [37]. Additionally, only a small number of nano PCMs suffer from leakage issues related to the solid-liquid phase transition. Different mechanical and chemical techniques are useful to prevent agglomeration to prepare homogeneous and long-term stable Nano-PCM for enduring domestic and industrial applications [38].

The integration nanoparticles into the PCM enhances the thermal conductivity, intensify charging -discharging rates when compared to the pure PCMs [39]. The highest electrical efficiency of 13 % and thermal efficiency of 68.4 % were achieved in an experimental investigation by Salem et al. [40] with water and/or an Al_2O_3/PCM mixture with varying nanoparticle concentrations in channels beneath the PV panel. Al-Waeli et al. [41] experimentally carried out an investigation by utilizing nano-PCM/nanofluid on a PVT system. They utilized paraffin wax as PCM and nano-SiC on both PCM and water and results found that the highest electrical efficiency for conventional PV and the PVT/nanofluid/nano-PCM was 7.1 % and 13.7 %, respectively, whereas the PV/T system achieved the highest thermal efficiency of 72 %. Abdelrazik et al. [42] investigated numerically using graphene nanoplatelets (GNP) with PCM and the outcome suggests that the PVT/nano-PCM (10wt%) exhibited the improvement in efficiency by 22 % in summer and 6.9 % in winter than conventional PV panels. Islam et al. [43] examined the impacts of nano-enhanced PCM on the PVT and reported that in Malaysian climatic conditions, the energy and exergy efficiencies reached their peak at 85.3 % and 12 %, respectively. Two-phase change material nano-emulsions were used by Liu et al. [44]. The module's overall thermal-equivalent energy efficiency averaged 84.41 % and peaked at 89.23 %. In a controlled environment, an electrical efficiency of 9.6 % and a thermal efficiency of 77.5 % were attained by Bassam

et al. [45] using nanofluid containing 0.6 vol% SiC and nano PCM containing 1 % SiC nanoparticles. However, the chemical stability analysis and characterization of nano particles integrated PCM have not been reported in their study. Incorporating aluminum metal foam with PCM resulted in a reduction of 13.2 % in PV surface temperature during an outdoor experiment done by Sharaf et al. [46]. PV-Alumina nano phase change material increases electrical efficiency by 8.1 %, according to research by Sheik et al. [47] that used alumina and silica nanomaterial with polyethylene glycol (PEG) 1000. The detailed investigation in relation to the chemical stability and thermal properties are not reported in their analysis.

The published literature shows that the incorporation of PCM at the back portion of the PV panel provides better efficiency than conventional PV panels. Furthermore, the utilization of nano PCM yields even greater efficiency compared to the PVT/PCM system. Table 1 shows the summary of recent research articles published on the nanomaterial-incorporated PCM employed in PVT systems. Based on the literature review, it is evident that the majority of research on PVT systems utilizes either PCM or nano PCM to enhance performance. Very few research works used hybrid nano PCM in their investigation. For example, the investigation of thermal management of the PVT using hybrid nanoparticles (CuO and Al_2O_3 with a 1.5 % by volume) and hybrid cooling mood was investigated by Gad et al. [48]. The study reported that the cooling of PV modules with hybrid nanoparticles achieved a maximum daily energy efficiency of 56.45 %, surpassing the conventional solar cell with PCM (SP31). However, the characterization of the hybrid nanoparticles and their stability analysis along with the analysis of RSM for optimizing the PVT/PCM and PVT/HNPCM systems were not reported in their study. The thermophysical properties of hybrid nano PCM were not reported in that literature either.

Built environment often refers to the constructed surroundings that serve as the backdrop for human activities, which range in size from residences and parks or greenery and frequently contain their essential infrastructure, especially energy networks. A possible significant development in the built environment, especially for building applications, is the combined application of PVT systems incorporation with hybrid nano-PCM (HNPCM). These arrangements increase total energy efficiency by combining the thermal energy production capabilities for heating purposes with the electrical generation capacity of PV panels [49,50]. Furthermore, the integration of renewable energy sources like Building Integrated Photovoltaic and PVT systems with incorporated HNPCM for improving the thermal and electrical performance facilitates the decarbonization of building energy systems and leads to the transition to green carbon building ambiance, due to their decentralized potential [51-53]. As a result, the investigation of this research goes further by analyzing the performance of the PVT system utilizing the HNPCM. The key contribution of this research is to characterize the HNPCM (Al_2O_3 and ZnO with 2 % concentration by weight with PCM) to examine the thermal stability and its suitability for storing thermal energy. The hybrid-nano/PCM samples are prepared and then their morphology, structure, thermal stability, thermal conductivity, and phase change behavior are carried out using SEM, DSC, TGA, FTIR analysis, and thermal conductivity measurements. In this investigation, Al_2O_3 and ZnO are incorporated in different concentrations with PCM to enhance its thermal conductivity and then used in the PVT system to examine the impact on their performance (electrical and thermal). The optimal concentration of the phase change material that maximizes thermal conductivity is utilized in the PVT system. Increased thermal conductivity of PCM enhances the efficiency of the photovoltaic-thermal system by enabling faster rates of heat storage and release. A serpentine copper pipe is inserted within the PCM so that water flowing through the pipe can absorb heat from the PCM and increase its heat storage capacity. In this study, hybrid nanoparticles of Al_2O_3 and ZnO with equal weights have been used and a comprehensive performance analysis of the PVT systems including HNPCM in comparison to only PV and PVT/PCM systems, has been performed.

Moreover, a prediction model is proposed based on response surface methodology (RSM) to exhibit the relations and impacts on response factors (dependent variable) of operating factors (independent variable) for the optimization of the systems (PVT/PCM and PVT/HNPCM) model. Then, the experimental findings were compared with the mathematical model results obtained by RSM analysis and optimum operating factors have been proposed for both the systems.

2. Methodology

2.1. Instrumentation and procedures

The schematic layout of this experimentation is illustrated in Fig. 1. In this process, four 20 W polycrystalline PV modules (similar model: POLY-20 W) were tested first for the inspection in consistency of power output and on the basis of the testing outcomes, three 20 W polycrystalline photovoltaic panel were used to convert solar energy into a useful form, shown in Fig. 2. The output shows negligible variations in the output power with respect to the solar irradiation. The detailed technical specification is reported in Table 2. The passing fluid (water) temperature through copper tube is measured at the point of entry and exit using a thermocouple (MASTECH MS6514). The programmable temperature sensor along with a microcontroller (specification in Table 3) is enclosed in a rectangular box and placed at the rear of the photovoltaic panel to measure the temperature of the panel. Another two programmable sensors were installed at the rear of the panel and middle of the container box of the PCM by using glue gun with high temperature resistance liquid adhesive to monitor the temperature of the PCM and HNPCM for second and third setup, shown in Fig. 2. A digital multimeter is utilized to measure the short circuit current of the PV panel with a pyranometer (Hukseflux LP02-LI19) for measuring solar irradiance. Two holes drilled into the top of the enclosure allowed hybrid nano PCM to be poured into the housing. Additionally, these perforations served as a breather to keep the pressure from rising. The amount of PCM was computed based on some parameters including the melting point temperature of PCM, the energy storage capacity of the PCM, the thermal conductivity of the PCM, and the estimated solar intensity. The experiments were conducted on sunny and fresh weather days with solar irradiation varying from 400 W/m^2 to 900 W/m^2 which was sufficient to provide sensible heat equivalent to the given mass of PCM and HNPCM up to the melting point temperature of PCM and HNPCM for the second and third setup as the observation was made for 1 hour. Based on the computation and consideration of those parameters, 2 kg of PCM was found to be the effective amount for being completely melted. The PCM container made of insulator material (plastic wood) was filled with 2 kg paraffin wax with hybrid nano-particles (specification in Table 4) with an identical concentration of 2 % (Al_2O_3 and ZnO) having a melting point temperature around 60.07 °C and closed tightly with a serpentine copper tube which has a perfect relation between the PV panel and pipe shown in Fig. 2. To stop liquid PCM from leaking, a rubber gasket sealed with sealant was positioned between the PV back and PCM enclosure and then tightened. Thermal energy storage is utilized with the PVT system to store thermal energy for domestic purposes.

2.2. Experimental configuration

The experimental procedures were carried out at Rajshahi University of Engineering and Technology, RUET campus on 26th April 2022, Rajshahi (latitude: 24°22′N, longitude: 88°36′E), Bangladesh. The experiments were conducted on sunny and fresh weather days with solar irradiation varying from 400 W/m^2 to 900 W/m^2. The ambient or room temperature was recorded at around 26 °C. The flow rate of water through the pipeline to extract heat from the PCM and HNPCM was kept at 0.0021 kg/s by using a water tap attached with the overhead tank and was monitored using flow rate sensor, shown in Fig. 2. In this experimentation procedure, three different cases have been examined includ-

Table 1
Recent studies on improving efficiency of PVT system.

System Configuration	Area	Cooling Methods	Thermal Storage PCM/Nano-PCM/Fin	System Efficiency		Year	References
				Electrical	Thermal		
Liquid-cooled PVT	Hong Kong	Passive Cooling (NPCM)	PVT/PCM-nano emulsion (melting point 29 °C or 38 °C)	–	84.41 % on average and 89.23 % by employing the nano-emulsion	2023	[44]
PVT/SiC-nano fluid/SiC-nano PCM (PVT M.F.N.F.N.PCM)	Malaysia	Passive cooling	PVT using a nanofluid circulation system and an inner-grooved micro fin tube encased in nano PCM	9.6 %	77.5 %	2023	[45]
PV/PCM/AMF	Egypt	Passive cooling	Aluminum metal foam (AMF) with PCM	10.5 % increment of electrical power	–	2022	[46]
PV nano-PCM	India	Passive Cooling (NPCM)	Polyethylene glycol (PCM) + (Alumina / Silica)	8.1, and 7.17 % than without cooling	–	2022	[47]
PV nano-PCMs	Pakistan	Passive Cooling (NPCM)	PT-58 PCM with (0.25, 0.5 wt%) MWCNT, graphene nanoplatelets and MgO	11.7 %, 12.10 % and 11.74 % than conventional PV	–	2021	[54]
PVT nano-PCM	Saudi Arabia	Compound Cooling	Eutectic of capric and palmitic acid, $CaCl_2{\cdot}6H_2O$, Paraffin wax as PCM+ GnP nanoparticles	6.9 % increase in winter, 22 % increase in summer	–	2020	[42]
PV/PCM with fin	Thailand	Passive Cooling (PCM+ fin)	Palm Wax as PCM in finned container	9.82 %	–	2020	[35]
PV/PCM	Iran	Passive Cooling (PCM)	Calcium chloride hexahydrate as PCM	24.68 % than conventional PV	–	2020	[33]
PVT/PCM	Malaysia	Water active cooling	Aluminum foil packets containing lauric acid as PCM	11.08 %	87.72 %	2019	[37]
PVT nano-PCM	Egypt	Compound cooling (Active+ Passive)	$CaCl_2{\cdot}6H_2O$ as PCM+Al_2O_3 nanoparticles	13 %	68.4 %	2019	[40]
PVT nano-PCM/ nanofluid	Malaysia	Compound Cooling	Paraffin wax	13.7 %	72 %	2019	[41]
PV-Water spray by nozzle	Italy	Water Active Cooling	–	13.6 %	–	2017	[55]
PVT/PCM	India	Compound Cooling	Paraffin wax RT-30	12.6–13.1 % increment	15.96–35.4 %	2017	[34]
PV-back surface water cooling	Saudi Arabia	Water Active Cooling	–	9 % increase in electrical efficiency	–	2013	[56]

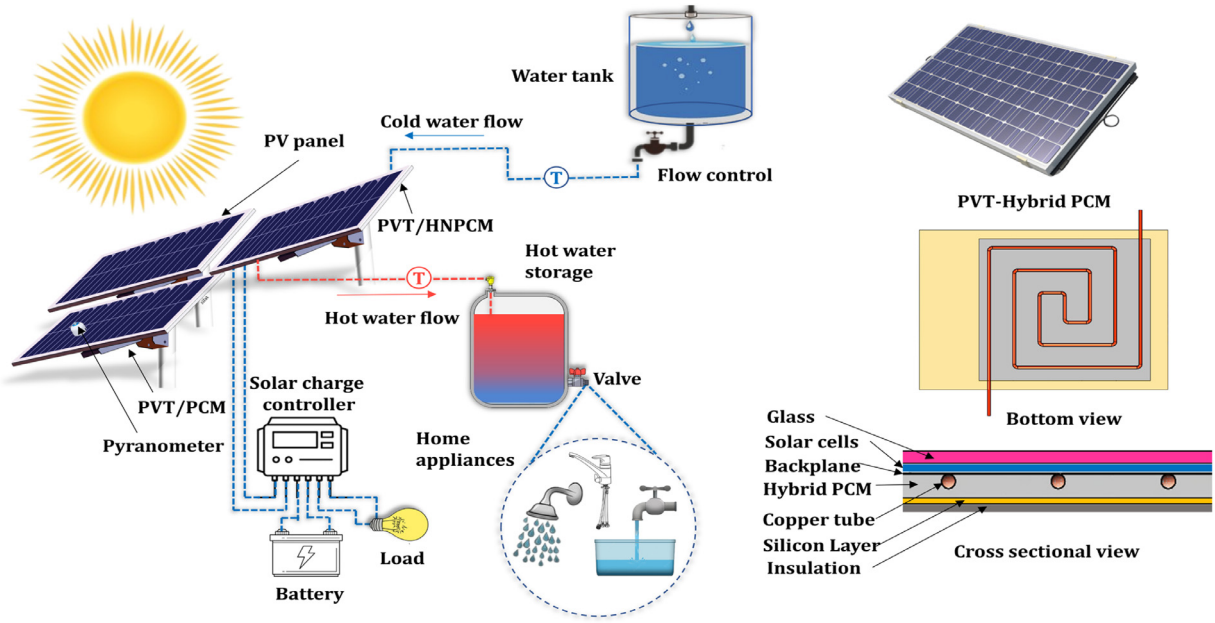

Fig. 1. Schematic layout of the experimental setup.

Fig. 2. Experimental setup of PVT hybrid nano-PCM (PVT/HNPCM) system.

Table 2
Specifications of photovoltaic panel.

Brand	Generic solar panel
Type	Polycrystalline
Model	POLY-20 W
Dimension	490 mm× 350 mm× 25 mm
Rated max. power (P_{max})	20 W
Tolerance	±3 %
Rated current (I_{mp})	1.15 A
Rated voltage (V_{mp})	17.4 V
Open circuit voltage (V_{oc})	22.4 V
Short circuit current (I_{sc})	1.23 A
Weight	1.3 kg
STC	1000 W/m^2, AM 1.5, 25 °C

Table 3
Specification of programmable sensor and microcontroller.

Parameters	Sensor Values	Microcontroller values
Model	Dsb18b20	NodeMCU ESP8266
Operating voltage	3–5 V	3.3V
Temperature range	−55 °C to +125 °C	−40 °C to +125 °C
Output resolution	9–12 bit	–
Accuracy	±0.5 °C	–
Conversion time	750 ms at 12bit	
Size	–	58 mm * 32 mm

ing (i) PV panel (Only photovoltaic panel), (ii) PVT/PCM system with water-flowing fluid, and (iii) PVT/hybrid nano-PCM (PVT/HNPCM, 2 % Al_2O_3, and 2 % ZnO) system with water-flowing fluid.

2.3. Preparation of the hybrid nano-PCM

The preparation of hybrid nano-PCM was carried out by using a two-step method in which the nanomaterials were dispersed into PCM. In this process, nanoparticles and paraffin wax were weighed at the right proportion by using the digital weighing machine. Then, the measured

Table 4
Thermo-physical characteristics of paraffin wax and nano-particles [57].

Thermo-physical Properties	Paraffin wax	Al_2O_3 nano particles	ZnO nano particles
Thermal conductivity	0.18 W/m K	17.65 W/m K	23.4 W/m K
Density	805 kg/m^3	3970 kg/m^3	5606 kg/m^3
Particle size	–	30 – 35 nm	40 – 50 nm
Specific heat	2150 J/kg K	525 J/kg K	514 J/kg K
Volume expansion	12.50%	–	
Particle shape	–	Spherical	Spherical
Purity	–	+99%	+99%
Temperature of transition	44 °C	–	–
Transitional interval	1 °C	–	–
Latent heat	−242 kJ	–	–

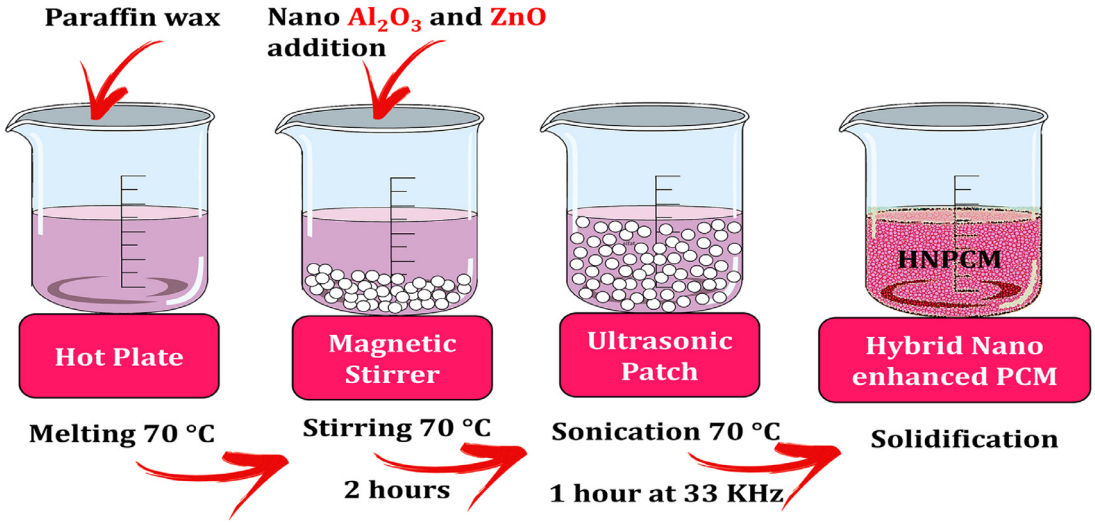

Fig. 3. Schematic diagram of two-step preparation method.

paraffin wax was melted in a beaker at 70 °C temperature and nano-additives (Al_2O_3 and ZnO) at the identical concentration of 2 % were dispersed into the wax and stirred at 70 °C for around 2 h by using the stirring machine. Then, the beaker was kept in an ultrasonic vibration machine above melting point temperature at 33 kHz frequency to have proper dispersion of nanoparticles into PCM for around 1 hour. At last, the sample was cooled at room temperature. The material preparation procedure is given as shown in Fig. 3.

2.4. Fabrication of pvt system

Aluminum oxide and Zinc oxide nanoparticles of 2 % are incorporated into 2 kg of paraffin wax. A serpentine copper pipe is imposed at the back side of the PV panel and then the hybrid nano-PCM is added and sealed. The mixture was sonicated in the ultrasonic bath and added to the panel. A hybrid nano-PCM with a serpentine copper tube is shown in Fig. 4.

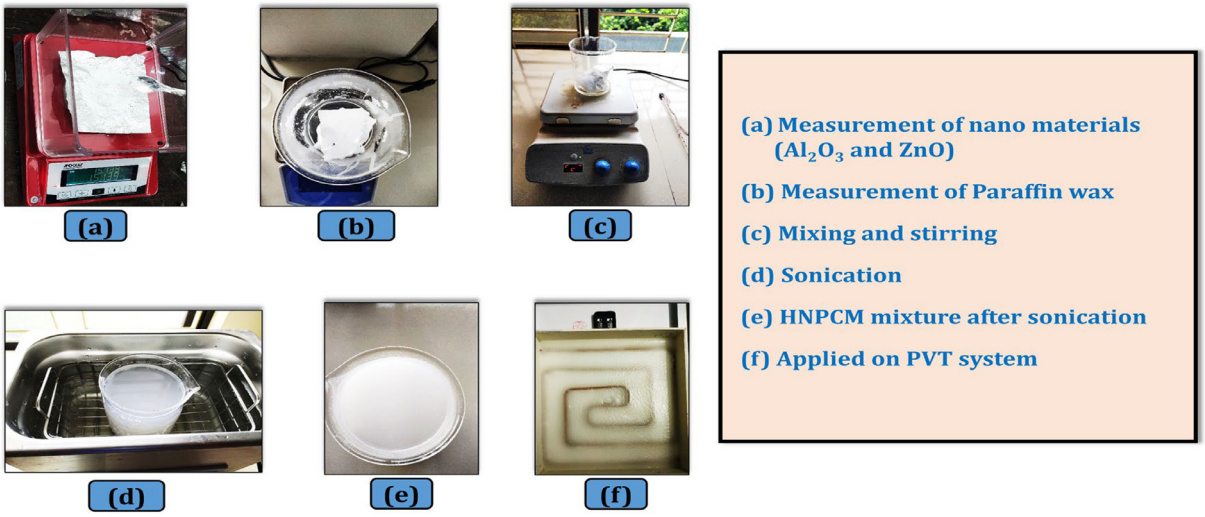

Fig. 4. Final preparation process for fabrication PVT system.

3. Characterization of hybrid nano-PCM

3.1. Chemical stability measurement

A PerkinElmer Spectrum Two-UATR is used to calculate the hybrid PCM/hybrid nanocomposites' Fourier transform infrared spectrum (FTIR). The integrated detector of the MIR TGS (15,000–370 cm^{-1}) detects spectra. The optimal scan range of 7800–450 cm^{-1} was covered by a scan at a speed of 0.2 cm s^{-1}. To investigate the chemical interactions of nano-ZnO, nano-Al_2O_3 particles, and paraffin, this analysis is crucial. Basically, for optimal effect, ZnO and Al_2O_3 nanoparticles should be dispersed finely inside the paraffin structure rather than reacting with the paraffin.

3.2. Morphological and structural characterization

Scanning Electron Microscopy measurements of the morphology and dimensions of the materials were carried out on a Zeiss (EVO-18) SEM. SEM micrographs are used to examine the size, shape, and dispersion of nanomaterials into the base material (Al_2O_3 and ZnO NPs in the PCM composite matrix). The samples had a gold coating to prevent charge accumulation, and an in-lens detector to provide information about the surface morphology of the samples. The images were taken using a low-resolution scanning technique to prevent the high energy electron from fusing paraffin [58].

3.3. Thermal stability analysis

The thermal stability of pure commercial grade PCM (paraffin) and hybrid PCM/ZnO-Al_2O_3 nanocomposites was examined by TGA analysis using the PerkinElmer TGA 4000. The samples were examined at 19.8 mL/min of ultra-high pure nitrogen gas flow, and 2.6 bar of gas pressure. A heating rate of 20 °C/min was used to get the desired temperature of 30 °C to 800 °C. In this experimentation process, Pyris Software was used to examine the acquired data. For the collection of data for each sample, a distinct procedure with a mass of 12 mg and a heating rate of 20 °C/min is maintained.

3.4. Thermal conductivity measurement

Using the DTC-25 thermal conductivity tester, the thermal conductivity of PCM and hybrid nano/PCM was determined, having a thermal conductivity range 0.1 to 20 W/mK and Accuracy ±3 % to 8 % depending on conductivity. The thickness of the specimen is maximum 1.25″ (32 mm) depending on thermal resistance and thin films down to 0.004″ (0.1 mm) is supported. A test specimen is secured between two polished metal surfaces while being compressed. The temperature of the upper surface is controlled. A calibrated heat flux transducer with a lower surface is joined to a heat sink that is liquid-cooled. Contact resistance is reduced to a minimum by using thermal interface pastes and applying a consistent pneumatic push to the test stack. The stack creates an axial temperature gradient when heat moves from the upper surface through the heat sink and test specimen. The temperature drop through the specimen may be measured thanks to temperature sensors inserted into the metal surfaces on each side of it. Following the attainment of thermal equilibrium, the output from the heat flux transducer is monitored along with the temperature difference across the specimen. The thermal conductivity is then determined using these numbers and the thickness of the specimen.

3.5. Phase change behavior

On the paraffin wax samples, a Differential Scanning Calorimetry (DSC) examination has been performed. A differential scanning calorimeter (Mettler-Toledo DSC822) is used to calculate the latent heat of fusion, heat capacity and melting temperature of the hybrid nano-PCM samples. The DSC cell is loaded with a sample amount of approximately 15–20 mg, and nitrogen is always utilized as a purge gas. Without removing them from the measurement crucible, three samples are placed into crucibles and evaluated sequentially over the course of several heating/cooling cycles.

3.6. Mathematical modelling

The PV module output electrical power is determined using the formula reported in Eq. (1). Furthermore, the Eq. (2) [59] can be used to determine the fill factor (FF).

$$\dot{E}_{el} = V_{oc} \times I_{sc} \times FF \tag{1}$$

$$FF = \frac{(V \times I)_{max}}{V_{oc} \times I_{sc}} \tag{2}$$

In the above equations, V_{oc} refers to the open circuit voltage, and I_{sc} refers to the short circuit current.

Therefore, the PV module efficiency is determined using the Eq. (3), whereby G is the amount of solar irradiance, A_c is the effective area of the PV panel.

$$\eta_{el} = \frac{E_{el}}{E_{sun}} = \frac{V_{oc} \times I_{sc} \times FF}{G \times A_c \times \tau_g \times \alpha_{cell}} \tag{3}$$

The thermal efficiency of the PV/T system can be obtained from the following relation [60]:

$$\eta_{th} = \frac{E_{th}}{E_{sun}} = \frac{m_f \times C_{p.f} \times \left(T_{f\ out} - T_{f\ in}\right)}{G \times A_c \times \tau_g \times \alpha_{cell}} \tag{4}$$

where m_f denotes the coolant mass flow rate, $C_{p.f}$ denotes the specific heat, $T_{f\ in}$ and $T_{f\ out}$ is the inlet and outlet temperature of the coolant, respectively.

The overall efficiency is written in the form [44],

$$\eta_{ov} = \eta_{el} + \eta_{th} \tag{5}$$

3.7. Regression modelling

RSM starts with the design of experiments (DOE) to define the operating and response factors and experiment strategy. Then, the experimentally obtained data will be utilized to derive a mathematical expression that exhibits the relation between the operating factors and response factors. In this section, some equations are employed to predict the relationship between the operating factors (independent variable) and response factors (dependent variable) of the PVT/PCM and PVT/HNPCM systems. In this study, daytime, solar intensity, and mass flow rate of water have been identified as operating factors and electrical efficiency, thermal efficiency, and overall efficiency have been selected as response factors. RSM provides the correlations for the response factors as a function of operating factors. The interaction effects of the operating factors on response factors are expressed as the linear and two-factor interaction (2FI) mathematical model which provides higher reliability for the prediction in both PVT/PCM and PVT/HNPCM systems. Eq. (6-11) provides the equations that present the interaction between operating factors and response factors in terms of coded factors obtained from ANOVA analysis.

For the PVT/PCM system

$$\begin{aligned}\text{Electrical efficiency, } \eta_{el} = {} & -84.67323 + (13.74436 \times A) + (0.065852 \times B) \\ & -(16,747.67940 \times \mathrm{C}) - -(0.013004 \times A \times B) \\ & -(2693.70935 \times A \times \mathrm{C}) + (67.43487 \times B \times \mathrm{C})\end{aligned} \tag{6}$$

$$\text{Thermal efficiency}, \eta_{th} = -202.99918 + (19.19688 \times A) + (0.289576 \times B) - (21,122.44351 \times C) - -(0.022608 \times A \times B) - (3794.71294 \times A \times C) + (91.22377 \times B \times C) \quad (7)$$

$$\text{Overall efficiency}, \eta_{ov} = -287.67241 + (32.94125 \times A) + (0.355428 \times B) - (37,870.12291 \times C) - -(0.035612 \times A \times B) - (6488.42229 \times A \times C) + (158.65863 \times B \times C) \quad (8)$$

For the PVT/HNPCM system

$$\text{Electrical efficiency}, \eta_{el} = -88.87176 + (13.61878 \times A) + (0.076367 \times B) - (15,801.74927 \times C) - -(0.013179 \times A \times B) - (2560.69186 \times A \times C) + (63.84559 \times B \times C) \quad (9)$$

$$\text{Thermal efficiency}, \eta_{th} = -235.49058 + (26.40171 \times A) + (0.306615 \times B) - (25,021.42556 \times C) - -(0.029368 \times A \times B) - (3485.78717 \times A \times C) + (91.15129 \times B \times C) \quad (10)$$

$$\text{Overall efficiency}, \eta_{ov} = -324.36233 + (40.02049 \times A) + (0.382982 \times B) - (40,823.17483 \times C) - -(0.042547 \times A \times B) - (6046.47903 \times A \times C) + (154.99688 \times BC) \quad (11)$$

Where A is the daytime, B is the intensity, and C is the mass flow rate.

3.8. Uncertainty estimation

In the experimental studies, a researcher should deal with a number of independent variables where it is crucial to ensure that the measurement of outcomes is free from errors. Some of these errors are systematic related to the used equipment, made by the researcher, and for the environmental impact. Cloud cover and humidity have an impact on photovoltaic panel performance. The voltage and current dropped due to high humidity. The average relative humidity over the course of the experiment was lower than 60 %. Furthermore, additional factors including wind speed, air-water vapor content, and the portion of the sky covered by clouds were not taken into account. In some cases, the error measurements can be figured out and resolved easily. On the other hand, some experimental outcomes don't correspond with our expectations and that doesn't indicate that those outcomes are worthless. The uncertainty values of the used equipment are given in Table 5.

To determine the errors in the measurement, following Eq. (12) can be used [61]:

$$W_R = \left[\left(\frac{\partial R}{\partial x_1} x_1\right)^2 + \left(\frac{\partial R}{\partial x_2} x_2\right)^2 + \ldots + \left(\frac{\partial R}{\partial x_n} x_n\right)^2\right]^{1/2} \quad (12)$$

Where W_R represents the total uncertainty of the equipment, R denotes the function of dependent variables and $(x_1, x_2, \ldots ., x_n)$ are the values of the uncertainty of the independent variables. Based on this equation, the values of uncertainty of the dependent variables can computed as follows:

Table 6
Uncertainty values of performance parameters.

Performance parameter	Uncertainty (%)
Electrical power	0.071
Electrical efficiency	1.4
Thermal power	0.5
Thermal efficiency	1.49
Total	**2.11**

The uncertainty values of electrical power are determined as follows:

$$W_{R_1} = \left[(0.05)^2 + (0.05)^2\right]^{0.5} = 0.071$$

The uncertainty values of electrical efficiency are determined as follows:

$$W_{R_2} = \left[(0.071)^2 + (1.4)^2\right]^{0.5} = 1.4$$

The uncertainty values of thermal power are determined as follows:

$$W_{R_1} = \left[(0.5)^2 + (0.04)^2\right]^{0.5} = 0.5$$

The uncertainty values of thermal efficiency are determined as follows:

$$W_{R_1} = \left[(1.4)^2 + (0.5)^2 + (0.04)^2\right]^{0.5} = 1.49$$

Total uncertainty measurements are determined as follows:

$$W_R = \left[(0.071)^2 + (1.4)^2 + (0.5)^2 + (1.49)^2\right]^{0.5} = 2.11$$

The value of total uncertainty of the experimental system is less than 3 % which refers to the high accuracy of the measurements and the values of uncertainty of each performance parameter are listed in Table 6.

4. Results and discussion

4.1. Chemical stability analysis

Adding nano-Al_2O_3 and ZnO particles at different mass percentages did not change the paraffin wax's peak wavelength. Medium symmetrical and strong asymmetrical stretching of the C–H vibration are exhibited in the sharp peaks at 2848 cm^{-1} and 2916 cm^{-1}. Other peaks also appear at 729 cm^{-1} and 1462 cm^{-1}, which could be explained by the scissor vibration of C–H molecules and the rocking skeleton vibration of C–C molecules, respectively. Fig. 5 shows the experimental findings for all four samples. There is no doubt that no additional distinct peaks were detected in the results of any of the specimens, which are shown to have the same kind of peaks related to the paraffin structure [37]. It proves that the ZnO and Al_2O_3 nanoparticles blended into the paraffin matrix uniformly without experiencing any chemical reactions. Because The weight percentage of paraffin is much larger than that of nano-ZnO and Al_2O_3 particles. The peaks of the ZnO and Al_2O_3 nanoparticles were suppressed, and the paraffin remained chemically stable without interacting with the nanoparticles. As a result, hybrid nanocomposites are practical for recurring cycles since they have strong chemical stability.

Table 5
Uncertainty values of equipment used in the measurement.

Equipment	Parameter	Independent variable uncertainty	Experimental uncertainty (%)
Pyranometer	Radiation	x_1	±1.4
Sensor (Dsb18b20)	Temperature	x_2	±0.5
Flowmeter	Water flow	x_3	±0.04
Digital Multimeter	Current and Voltage	x_4	±0.05

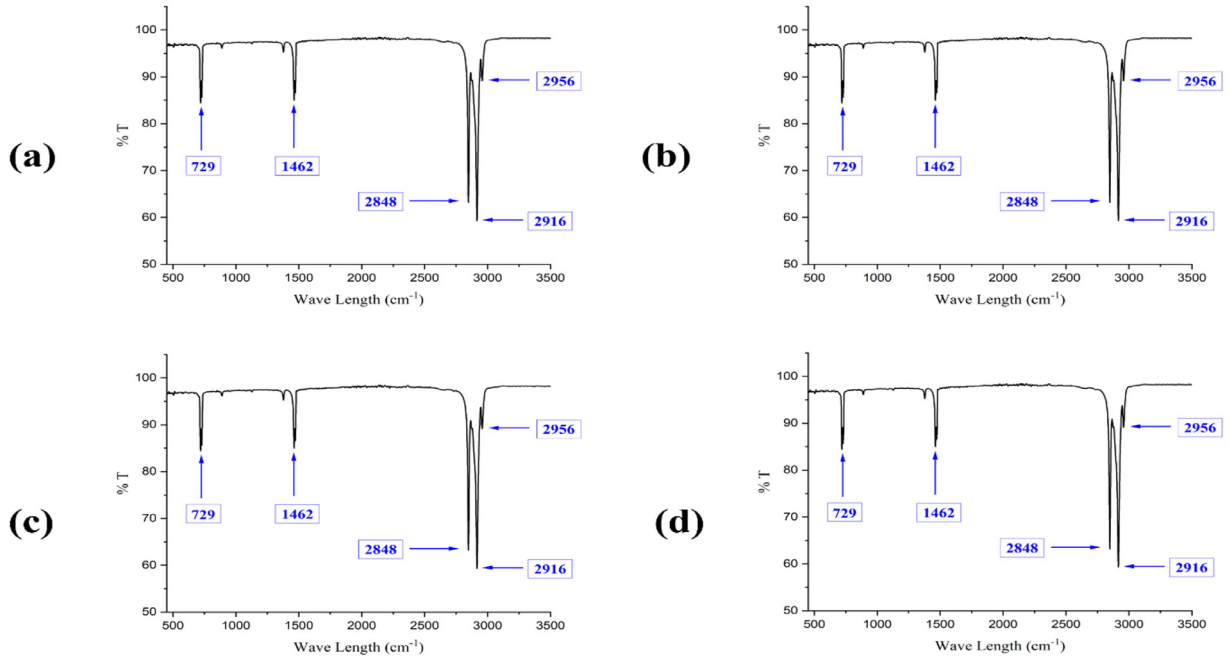

Fig. 5. FTIR results of the (a) Pure paraffin (b) 0.5 % Hybrid nano PCM (c) 1 % Hybrid nano PCM (d) 2 % Hybrid nano PCM.

4.2. Morphological and structural analysis

The SEM images Fig. 6 **(b–d)**, shows the dispersion of hybrid nano-particles into the paraffin matrix and the homogenous character of the hybrid nano-PCM at low mass fractions. It has been established as a proof that the nanoparticles created a strong physical interaction with the paraffin matrix, an interaction that was observed to grow even stronger with the increase in hybrid nanoparticle mass. Fig. 6**(b)** displays slight difference from Fig. 6**(a)** due to the presence of 0.5 % of hybrid nano-particles. The presence of light surface proves the availability of hybrid nano-particles in the PCM which grows with the percentage increment of hybrid nano-particles into the PCM, shown in Fig. 6**(c)**. The slightly scattering dispersion of hybrid nano-particles seems to be observed in Fig. 6**(c)** and tends to be agglomerated with the percentage increment of hybrid nano-particles into the PCM, shown in Fig. 6**(d)**. The Van der Walls forces between the nanoparticles and Brownian mo-

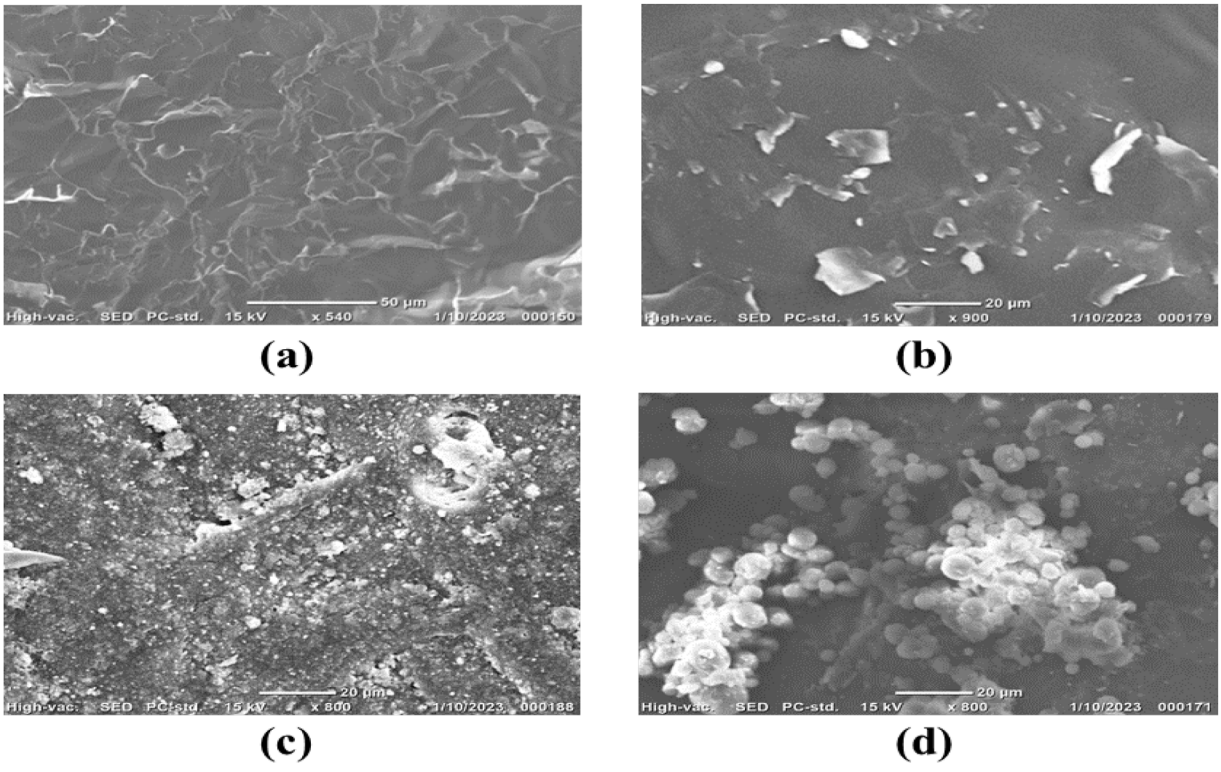

Fig. 6. SEM images of (a) Pure PCM (b) 0.5 % Hybrid nano-PCM (c) 1 % Hybrid nano-PCM (d) 2 % Hybrid nano-PCM.

tion, on the other hand, may be largely blamed for the agglomeration's tendency to develop when the mass of nanoparticles is increasing [58]. Nevertheless, in this experiment, all of the generated samples, with the exception of the sample containing 2 % of hybrid nanoparticles, showed superior physical contact without significant agglomeration, shown in Fig. 6**(d)**. That was mostly due to the adequate sonication that was provided throughout their preparation.

4.3. Thermal stability analysis

Thermal stability indicates the ability of each sample to withstand high temperatures without degradation. The thermal stability of hybrid nano-PCM (HNPCM) refers to how fast the mass of the sample vanishes against applying temperature. Fig. 7 exhibits the thermogravimetric analysis (TGA) of HNPCM with different mass percentages for the temperature range varying from 30 °C to 800 °C. It is evident that the samples with mass fractions of hybrid nanoparticles of 0 %, 0.5 %, 1 %, and 2 %, respectively, showed that their thermal deterioration began at approximately the same temperature, which is 260 °C. Afterward, 2 % of the hybrid nano-PCM sample seemed to be degraded at a faster rate than the other samples. On the contrary, after some point at 400 °C temperature pure paraffin and 0.5 % HNPCM were found to be degraded more rapidly than other remaining samples. At 500 °C, there was no remained residual mass for the samples pure PCM and 0.5 % HNPCM but the 6 % and 9 % residual mass still remained for the samples 1 % and 2 % respectively at the same temperature which indicates higher thermal stability for 2 % sample than others at higher temperature. 2 % mass of hybrid nano-particles seemed to have lower degradation at higher temperatures. The results obtained from this analysis are comparable to PCM behavior as observed by Tang et al. [62]. HNPCM mass loss has little impact because of the small percentage of hybrid nanomaterials in the PCM, and the disintegration processes primarily behave as pure PCM. The thermal stability of PCM may be affected if the concentration of hybrid nano-particles reaches higher levels, such as at least 10 mg [63]. The rise in temperature between 30 °C and 800 °C does not cause the HNPCM to degrade. The HNPCM has little mass loss throughout this range because of the rising temperature [64]. The stability of pure PCM lasts until its breakdown. In this temperature range, PCM breaks down in its microcapsules and constituent parts. Following the breakdown of the resulting components, the microcapsules degrade more gradually. In this testing temperature range (30 °C - 800 °C), 2 % of HNPCM are still found to have a residual mass than others at higher temperatures. So, this sample exhibited better thermal stability at higher temperatures than others.

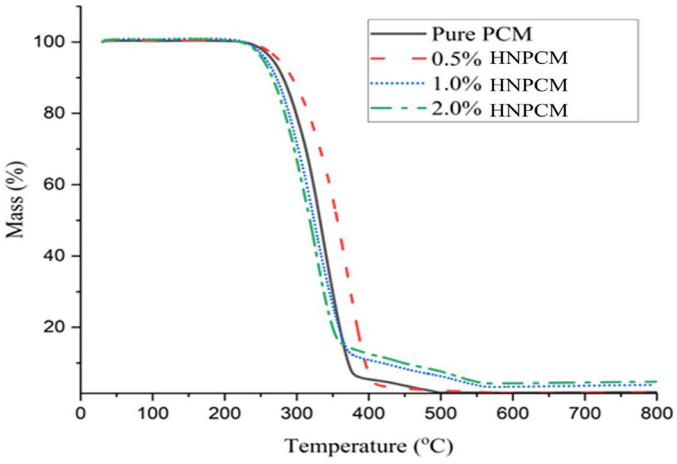

Fig. 7. TGA curve of pure paraffin and hybrid PCM/ ZnO-Al_2O_3 nanocomposites.

4.4. Thermal conductivity analysis

It has been found that adding 0.5 %, 1 %, and 2 % mass of hybrid nanoparticles to paraffin increases its thermal conductivity from 1.54 W/mK to 1.92 W/mK, 1.98 W/mK, and 2.18 W/mK, respectively. Pure paraffin has a thermal conductivity of 1.54 W/mK. With the increase in the mass of hybrid nanoparticles in paraffin, there is an enrichment in thermal conductivity that appears to be non-linear. The thermal conductivity has improved because convective heat transfer was increased more than conductive heat transfer by Brownian motion by using hybrid nanoparticles combined within paraffin [58], and this was the main driver of the base material's heat transfer rate amplifying noticeably. The experimental thermal conductivity of paraffin and hybrid nanoparticles with curve fittings are presented in Fig. 8**(a)**. From the curve fittings, the mathematical model of the thermal conductivity of hybrid nanoparticle samples (k) and the mass percentage of the hybrid nanoparticles (x) can be determined as follows:

$$k = 0.3467x^3 - 1.16x^2 + 1.2533x + 1.54 \quad (13)$$

The correlation coefficient of the above equation has reached to the value of unity which represents the good fit of data in the regression model.

Fig. 8**(b)** provides an interpretation of the percentage increase in the PCM's thermal conductivity resulting from the hybrid nanoparticle loading. The inclusion of nanoparticles caused a steady enhancement in thermal conductivity. The percentage increase for 0.5 %, 1 %, and 2 % mass of hybrid nanoparticles with PCM is 24.68 %, 28.57 %, and 41.56 % respectively. Fig. 8**(b)** shows that the slope appears to be lessened following the addition of 1.0 mass of nanoparticles. When they dispersed copper nanoparticles in paraffin, Similar patterns of change in thermal conductivity were found by Lin and Al-Kayiem [65]. They claim that the reduced slope in the magnitude of thermal conductivity at the upper mass fractions can be explained by the higher mass percentage of nanoparticles in the base material, which is caused by the predominate cohesive forces and goes beyond a threshold value.

4.5. Phase change behavior analysis

The curves exhibit the changes in thermal properties such as melting point and latent heat capacity of paraffin and Hybrid-nano paraffin. Two peaks have appeared in the DSC curves of the samples in Fig. 9. The materials' solid-liquid phase transition is represented by the longer main peak, while their solid-solid phase transition is represented by the smaller minor peak. Table 7 exhibits that the melting points and total latent heat of capacity for pure paraffin and HNPCMs saturated with paraffin in mass ratios of 99.5 %, 99 %, and 98 %. The melting point of 0.5 %, 1 %, and 2 % hybrid nano-PCMs were smaller than that of pure paraffin as 0.68, 1.04, and 1.49 °C, respectively. Furthermore, total latent heat capacity (solid-solid and solid-liquid phase change) of 0.5 %, 1 %, and 2 % HNPCMs were lower 1.02 %, 1.79 %, and 2.38 %, respectively, than that of pure paraffin. The latent heat capacity decreased as the mass percentage of hybrid nanomaterials increased, suggesting that the values of HNPCMs are nearly equal when the latent heat value of pure paraffin is multiplied by its mass fractions. The 2 % HNPCM has the lowest melting point and an adequate latent heat capacity (228.93 kJ/kg) for use with the PVT system. It is evident that Al_2O_3 and ZnO nanoparticles were deliberately mixed into paraffin, significantly lessening the melting point. It implies that the Al_2O_3 and ZnO nanoparticles continued to serve as nucleation agents and prevented the paraffin wax from supercooling. Nevertheless, the latent heat of pure paraffin wax decreased according to the mass percent of Al_2O_3 and ZnO.

4.6. Response surface methodology

Researchers frequently utilize the method of RSM for predicting and optimizing the interaction of operating factors (independent variable)

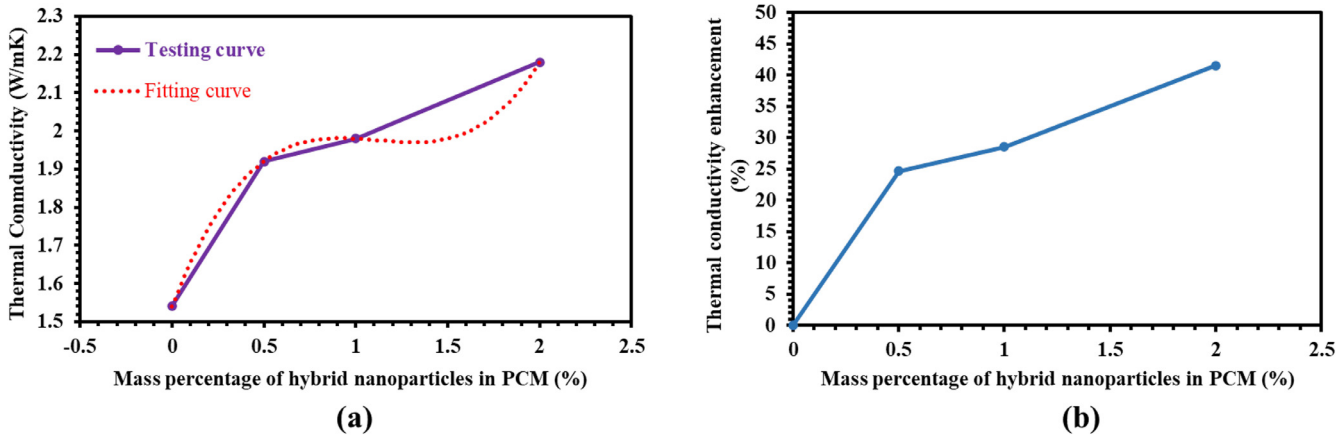

Fig. 8. (a) Thermal conductivity improvement of hybrid nanocomposites with respect to increasing mass percentage of hybrid nanoparticles, (b) Percentage thermal conductivity improvement of hybrid nanocomposites with respect to increasing mass percentage of hybrid nanoparticles.

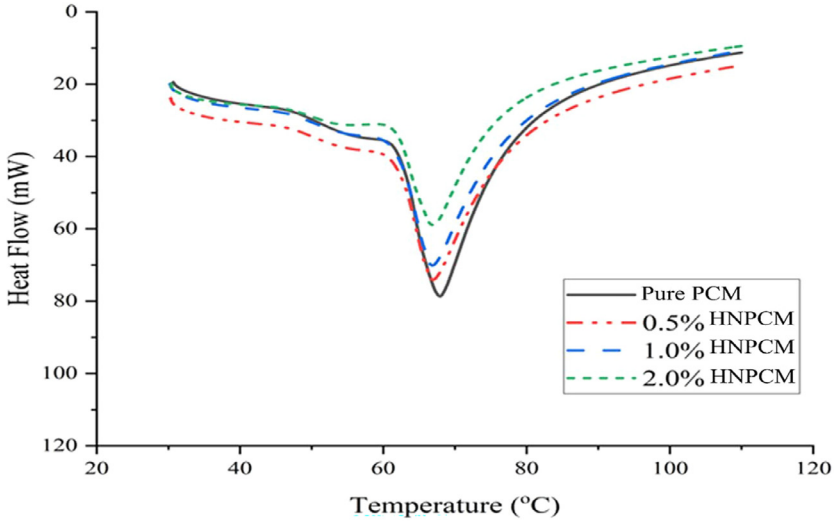

Fig. 9. DSC results of nano- Al_2O_3 and ZnO /paraffin PCM samples.

Table 7
Melting point and total latent heat of capacity for pure PCM and hybrid nano-PCMs.

Material	Melting point (˚C)	Total latent heat capacity (kJ/kg)
Pure PCM	61.56	234.52
99.5 wt% PCM and 0.5 wt% hybrid nano material	60.88	232.13
99 wt% PCM and 1 wt% hybrid nano material	60.52	230.32
98 wt% PCM and 2 wt% hybrid nano material	60.07	228.93

with the response factors (dependent variable). It uses statistics and mathematical models to develop, optimize, and improve the experimental system, permitting to determine the optimum parameter with a short number of runs. Initially, this method was popular for empirical studies. However, this has been extensively used in numerical studies recently due to its ability to reduce long experimental time and computational cost with its convenience such as predicting and optimizing the nonlinear system [66].

In this method, to obtain the interaction between the operating factors and response factors, a linear and two-factor interaction (2FI) mathematical model is utilized due to its higher reliability for the prediction model, reduction of the model variance, and selection of the best model. A general linear and 2FI model is explained by the following Eq. (14) [67]:

$$Y = \beta_0 + \sum_{i=1}^{n} \beta_i x_i + \sum_{i}^{n} \sum_{j}^{n} \beta_{ij} x_i x_j, \; i < j \tag{14}$$

Where Y represents the response of the model, n denotes the total number of factors, x denotes the independent variable, β_0 represents the constant coefficient, β_i is the linear regression coefficient of i^{th} factor, β_{ij} denotes the interaction of i^{th} and j^{th} factors. There are several designs available for the RSM method including the Box-Behnken-Doehlert and Central Composite Design (CCD) [66]. Central Composite Design (CCD) is selected for this study due to its high-quality prediction ability and generalization of the quadratic model. The statistical significance and the validation of the model is determined by the analysis of variance (ANOVA). The statistical significance of the model is computed by the F-value and P-value. The F-value indicates the measurement of data variance and high F-value is preferable for the significance of the model. The P-value should be less than 0.05 for the significance of the model [68,69].

4.6.1. Prediction model

This section uses a few equations to show how the response factors (dependent variable) and operating factors (independent variable) for

Table 8
ranges of operating factors for Eqs. (6)-11.

Operating factors	Value	Unit
Day Time (A)	$9 \le A \le 15$	AM/PM
Solar intensity (B)	$621 \le B \le 826$	W/m^2
Mass flow rate (C)	$0.00159 \le C \le 0.0025$	kg/s

the PVT/PCM and PVT/HNPCM systems relate to one another. Electrical efficiency, thermal efficiency, and overall efficiency are selected as response factors. On the other hand, solar intensity, daytime, and mass flow rate are regarded as operating factors. RSM provides the correlation between the response factors and operating factors and response factors are regarded as the function of operating factors. The equation exhibits the interaction effects of operating factors on responses. The quadratic polynomial equations are obtained for the prediction of responses by considering all the terms for the PVT/PCM and PVT/HNPCM systems. The F and P values of the ANOVA test are crucial to evaluate the importance of any regression model for each of the responses. It determines the acceptability of any regression model. It is seen from the published literature that lower P values and higher F values indicate the higher significance of the regression model. The regression model is regarded as the significance model for the value of P which is less than 0.05 [68,69]. The summary of the model fit-sequential model for each response (electrical, thermal, and overall) for both the PVT/PCM and PVT/HNPCM systems is presented in Tables 9-14. The Eq. (6-11), in terms of coded factors to satisfy the conditions presented in Table 8.

4.6.2. Interaction effect of variables on electrical efficiency

Fig. 10**(a-c)** and Fig. 10**(d-f)** exhibit the interaction of different operating factors on electrical efficiency for the PVT/PCM and PVT/HNPCM systems. It shows the variation of electrical efficiency in terms of intensity vs daytime, mass flow rate vs intensity, and mass flow rate vs daytime for both systems. **Fig. (a-f)** shows that the electrical efficiency enhances with the increment of solar intensity for both the systems (PVT/PCM and PVT/HNPCM) because the slight increment in solar intensity enhances the electrical power output. From Eq. (3), it is seen that the enhancement of electrical power output increases electrical efficiency. It is also apparently seen from both systems (PVT/PCM and PVT/HNPCM) that the mass flow rate of the working fluid has a positive impact on electrical efficiency. The enhancement of the mass flow rate of working fluid through the thermal collector indirectly affects the cooling of the PV panels which results in declination of cell temperature. The efficiency of PV panels declines with the increment of cell temperature [18].This results in significant improvement of the electrical efficiency of PV panels. However, the other operating factor of daytime has an effect on the variation of responses for both the PVT/PCM and PVT/HNPCM systems. It is seen from the experimental Fig. 17 that the electrical efficiency boosts up till the solar radiation rises up and the graph of RSM exhibits a similar trend with the variation of daytime parameter. With the increment of solar intensity with respect to the daytime operating factors also increases the electrical efficiency.

4.6.3. Interaction effect of variables on thermal efficiency

Fig. 11**(a-c)** and Fig. 11**(d-f)** exhibit the interaction of different operator factors on thermal efficiency for the PVT/PCM and PVT/HNPCM systems. The thermal efficiency of PVT/PCM and PVT/HNPCM systems measures how much the systems will convert the solar energy into a useful form of thermal gain. It is obvious from the RSM graphs that the highest mass flow rate (m_f) of working fluid exhibits higher thermal efficiency for both systems (PVT/PCM and PVT/HNPCM). This is due to the fact that the values of thermal efficiency is a function of the mass flow rate of the working fluid as presented in Eq. (4) and the better contact between the PCM layer and the upper layer of working fluid is responsible for extracting more heat from PCM layer to the working fluid which ameliorates the outlet temperature of the working fluid resulting the higher thermal power output. Higher thermal output refers to the higher thermal efficiency, from Eq. (4). The other operating factor of solar intensity has also a positive impact on thermal efficiency. The slight increment of solar intensity increases the thermal efficiency. This is due to the fact that it allows the PCM or HNPCM layer to extract more heat and melts rapidly. Hence, it enhances the outlet temperature of the working fluid resulting in higher thermal efficiency. However, there is a noticeable variation in thermal efficiency with the changing of daytime operating factor for both the PVT/PCM and PVT/HNPCM systems and the positive changes in thermal efficiency depends on the variation of solar intensity with respect to daytime.

4.6.4. Interaction effect of variables on overall efficiency

Fig. 12**(a-c)** and **(d-f)** exhibit the interaction of different operator factors on overall efficiency for the PVT/PCM and PVT/HNPCM systems. Overall efficiency is the summation of electrical and thermal efficiency. The slight increment of solar intensity enhances both electrical and thermal efficiency which is then results in higher overall efficiency. Hence, Fig. 12**(a-c)** and **(d-f)** show the enhancement of the overall efficiency with the increment of solar intensity. There is no variation in electrical efficiency with the changes in the mass flow rate of working fluid but it has a significant impact on thermal efficiency. Fig. 12**(a-c)** and **(d-f)** exhibit that the overall efficiency enhances with the increment of the mass flow rate of the working fluid. This is due to the fact that the increment in the mass flow rate of working fluid results in an increase in thermal efficiency, shown in Fig. 11**(a-c).** it is also seen from the RSM graphs that the operating factor of daytime has a positive impact on the overall efficiency till the solar intensity remains in an increasing trend with respect to the daytime operating factor. This is due to the fact that with the increment of solar intensity, both the electrical and thermal efficiency increase which in result to improve the overall efficiency.

4.6.5. Diagnostic analysis

Different diagnostic plots for the responses can be utilized to evaluate the statistical adequacy of the model. To check the adequacy of prediction model presented by RSM can be attained by analysis of different diagnostic plots. These plots can be fragmented into two categories including the plots based on Hat matrix and residuals. Among them, predicted versus actual plot has been created by Design Expert software which evaluates the adequacy of predicted values with the actual experimental values, presented in Fig. 13 and Fig. 14 for PVT/PCM and PVT/HNPCM systems.

Table 9
Summary of model fit sequential model of electrical efficiency for PVT/PCM system.

Source	Sum of Squares	df	Mean Square	F-value	P-value	Adjusted R^2	Predicted R^2	
Mean vs Total	3372.39	1	3372.39					
Linear vs Mean	53.22	3	17.74	11.34	0.0005	0.6459	0.3070	**Suggested**
2FI vs Linear	17.25	3	5.75	13.59	0.0005	0.9042	–	**Suggested**
Quadratic vs 2FI	2.20	1	2.20	8.96	0.0135	0.9444	–	**Aliased**
Residual	2.46	10	0.2455					
Total	**3447.52**	**18**	**191.53**					

Table 10
Summary of model fit sequential model of electrical efficiency for PVT/HNPCM system.

Source	Sum of Squares	df	Mean Square	F-value	P-value	Adjusted R^2	Predicted R^2	
Mean vs Total	3519.88	1	3519.88					
Linear vs Mean	58.12	3	19.37	12.32	0.0003	0.6664	0.3457	**Suggested**
2FI vs Linear	17.75	3	5.92	15.26	0.0003	0.9178	–	**Suggested**
Quadratic vs 2FI	2.27	1	2.27	11.41	0.0070	0.9577	–	**Aliased**
Residual	1.99	10	0.1992					
Total	**3600.02**	**18**	**200.00**					

Table 11
Summary of model fit sequential model of thermal efficiency for PVT/PCM system.

Source	Sum of Squares	df	Mean Square	F-value	P-value	Adjusted R^2	Predicted R^2	
Mean vs Total	28,948.99	1	28,948.99					
Linear vs Mean	511.07	3	170.36	34.02	<0.0001	0.8535	0.7320	**Suggested**
2FI vs Linear	52.93	3	17.64	11.30	0.0011	0.9543	–	**Suggested**
Quadratic vs 2FI	7.56	1	7.56	7.87	0.0186	0.9719	–	**Aliased**
Residual	9.61	10	0.9608					
Total	**29,530.17**	**18**	**1640.56**					

Table 12
Summary of model fit sequential model of thermal efficiency for PVT/HNPCM system.

Source	Sum of Squares	df	Mean Square	F-value	P-value	Adjusted R^2	Predicted R^2	
Mean vs Total	37,489.61	1	37,489.61					
Linear vs Mean	685.99	3	228.66	33.90	<0.0001	0.8531	0.7214	**Suggested**
2FI vs Linear	87.28	3	29.09	44.74	<0.0001	0.9848	–	**Suggested**
Quadratic vs 2FI	4.25	1	4.25	14.60	0.0034	0.9937	–	**Aliased**
Residual	2.91	10	0.2907					
Total	**38,270.04**	**18**	**2126.11**					

Table 13
Summary of model fit sequential model of overall efficiency for PVT/PCM system.

Source	Sum of Squares	df	Mean Square	F-value	P-value	Adjusted R^2	Predicted R^2	
Mean vs Total	52,082.71	1	52,082.71					
Linear vs Mean	875.22	3	291.74	24.48	<0.0001	0.8056	0.6339	**Suggested**
2FI vs Linear	130.59	3	43.53	13.22	0.0006	0.9463	–	**Suggested**
Quadratic vs 2FI	17.92	1	17.92	9.79	0.0107	0.9701	–	**Aliased**
Residual	18.30	10	1.83					
Total	**53,124.73**	**18**	**2951.37**					

Table 14
Summary of model fit sequential model of overall efficiency for PVT/HNPCM system.

Source	Sum of Squares	df	Mean Square	F-value	P-value	Adjusted R^2	Predicted R^2	
Mean vs Total	63,984.18	1	63,984.18					
Linear vs Mean	1108.14	3	369.38	25.61	<0.0001	0.8129	0.6391	**Suggested**
2FI vs Linear	183.63	3	61.21	36.85	<0.0001	0.9784	–	**Suggested**
Quadratic vs 2FI	12.73	1	12.73	22.97	0.0007	0.9928	–	**Aliased**
Residual	5.54	10	0.5542					
Total	**65,294.23**	**18**	**3627.46**					

4.6.6. Optimization of operating factors

The single-objective and multi-objective optimization are implemented using RSM to obtain the optimum values of operating factors as well as the predicted response at different level of goals for both PVT/PCM and PVT/HNPCM systems as below:

4.6.6.1. Single-objective optimization. The single-objective optimization is utilized to determine the optimum values of operating factors on the performance of the response factors for both PVT/PCM and PVT/HNPCM systems. In this optimization process, only one parameter is optimized while the others remain unchanged. To obtain the optimum values, three single-objectives are considered, including (a) to maximize only electrical efficiency, (b) to maximize only thermal efficiency, and (c) to maximize only overall efficiency. For having the single-objective optimization, it has been assumed that only one parameter is optimized while other parameters are not optimized. The optimum values of operating factors for each goal single-objective optimization are tabulated in Tables 15 and 16. The values of desirability have been observed close to the value of unity which indicates that the predicted responses remain in the desirable range.

4.6.6.2. Multi-objective optimization. the multi-objective optimization is employed by using the RSM to attain the optimum values of operating factors on the response factors for both PVT/PCM and PVT/HNPCM systems with four different goals, including (a) to maximize electrical and thermal efficiency, (b) to maximize thermal and overall efficiency, (c) to maximize electrical and overall efficiency, (d) to maximize electrical, thermal, and overall efficiency. During the optimization process, all the performance parameters are assumed to have equal importance and weights. The desirability approach is utilized to obtain the opti-

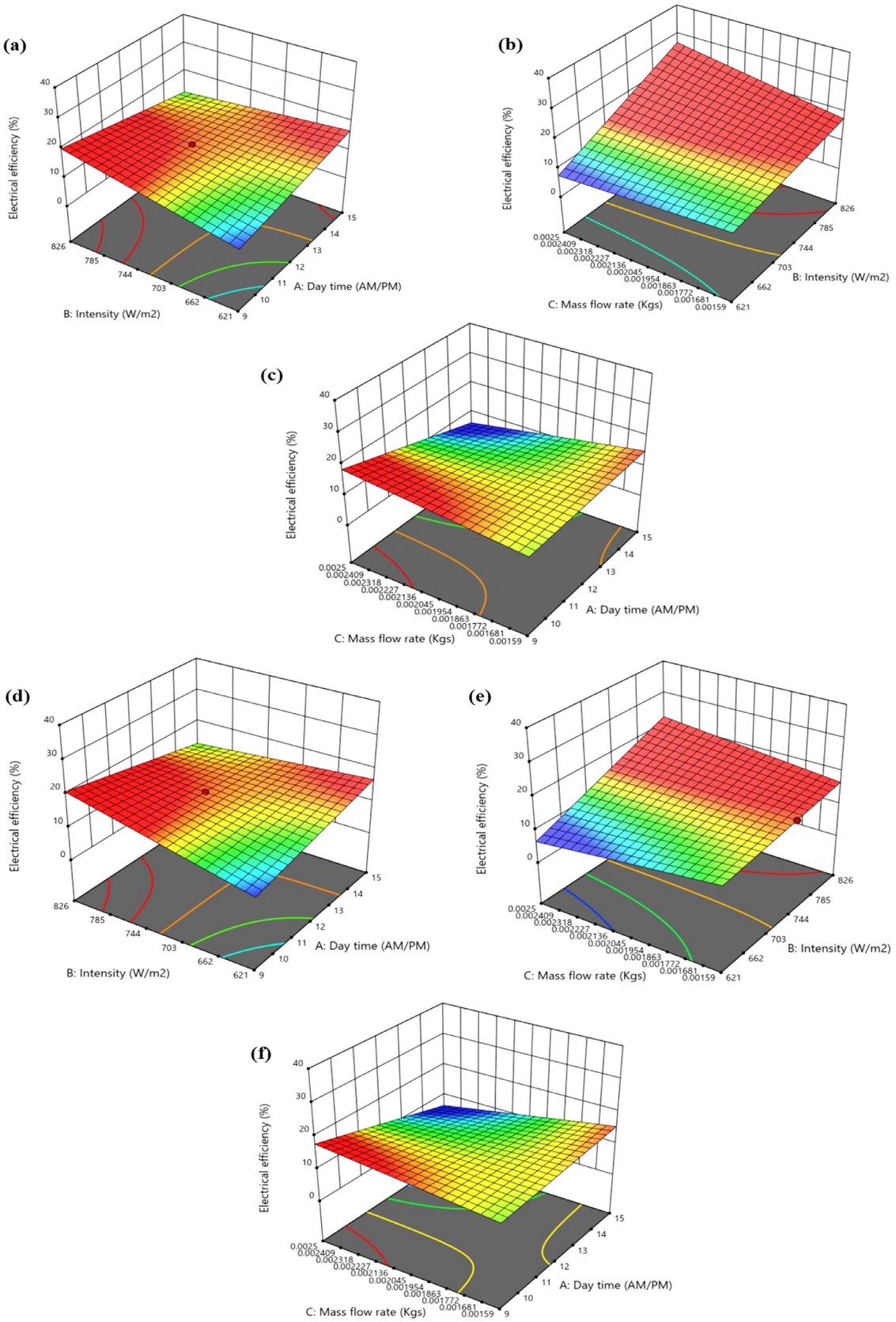

Fig. 10. (a-c). Effect of variables on electrical efficiency in PVT/PCM system. (d-f). Effect of variables on electrical efficiency in PVT/HNPCM system.

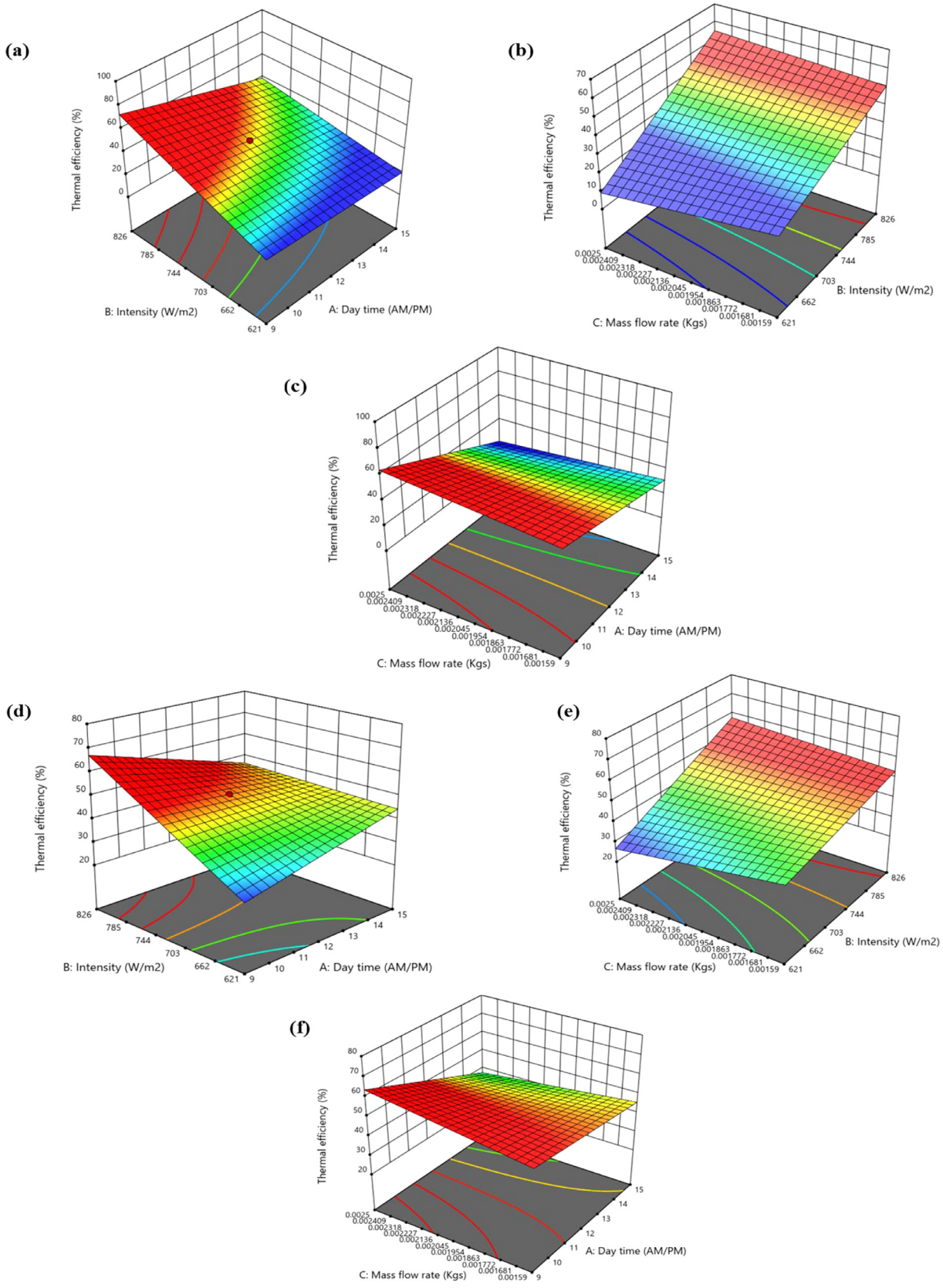

Fig. 11. (a-c). Effect of variables on thermal efficiency in PVT/PCM system.
(d-f). Effect of variables on thermal efficiency in PVT/HNPCM system.

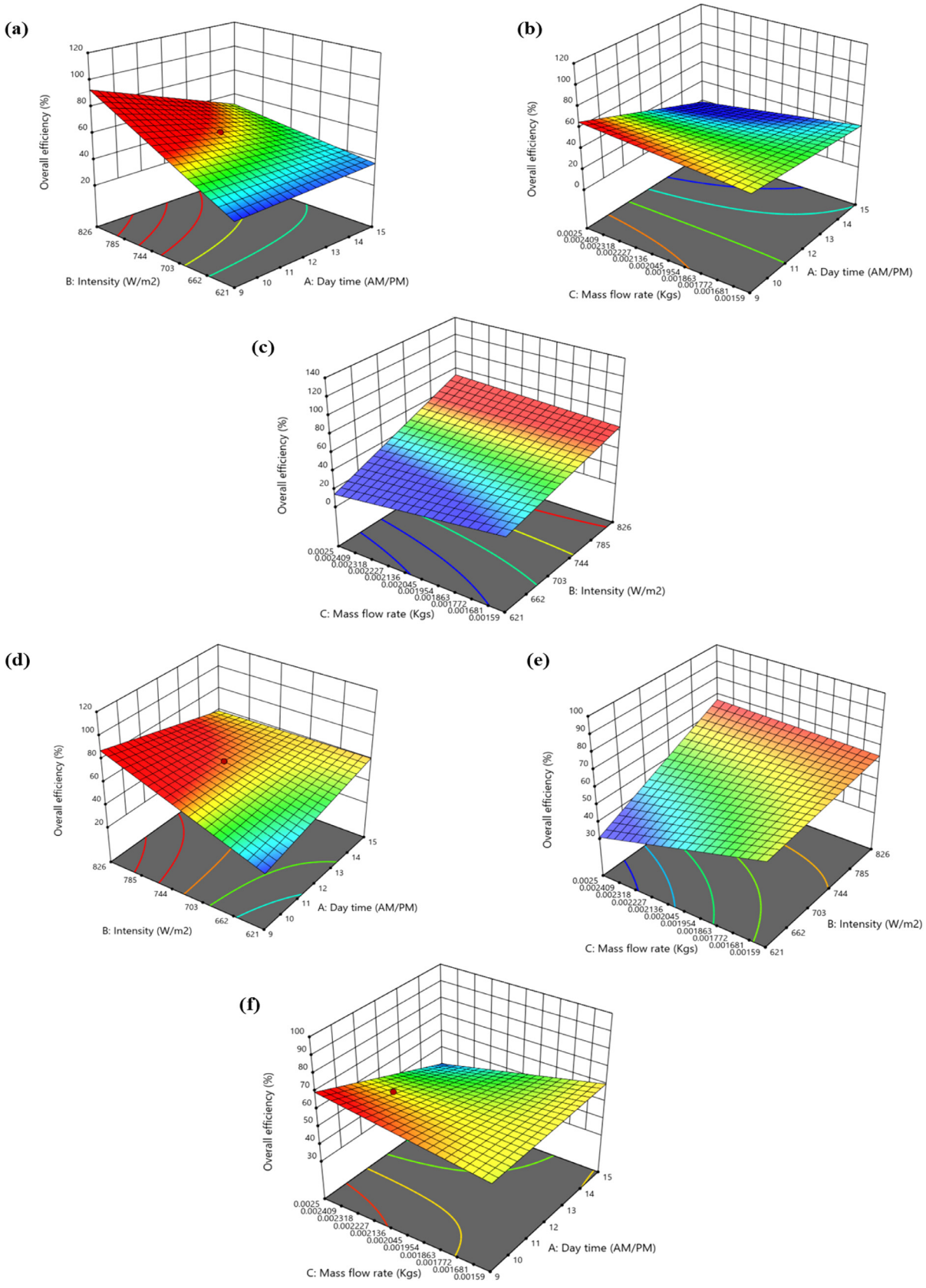

Fig. 12. (a-c). Effect of variables on overall efficiency in PVT/PCM system.
(d-f). Effect of variables on overall efficiency in PVT/HNPCM system.

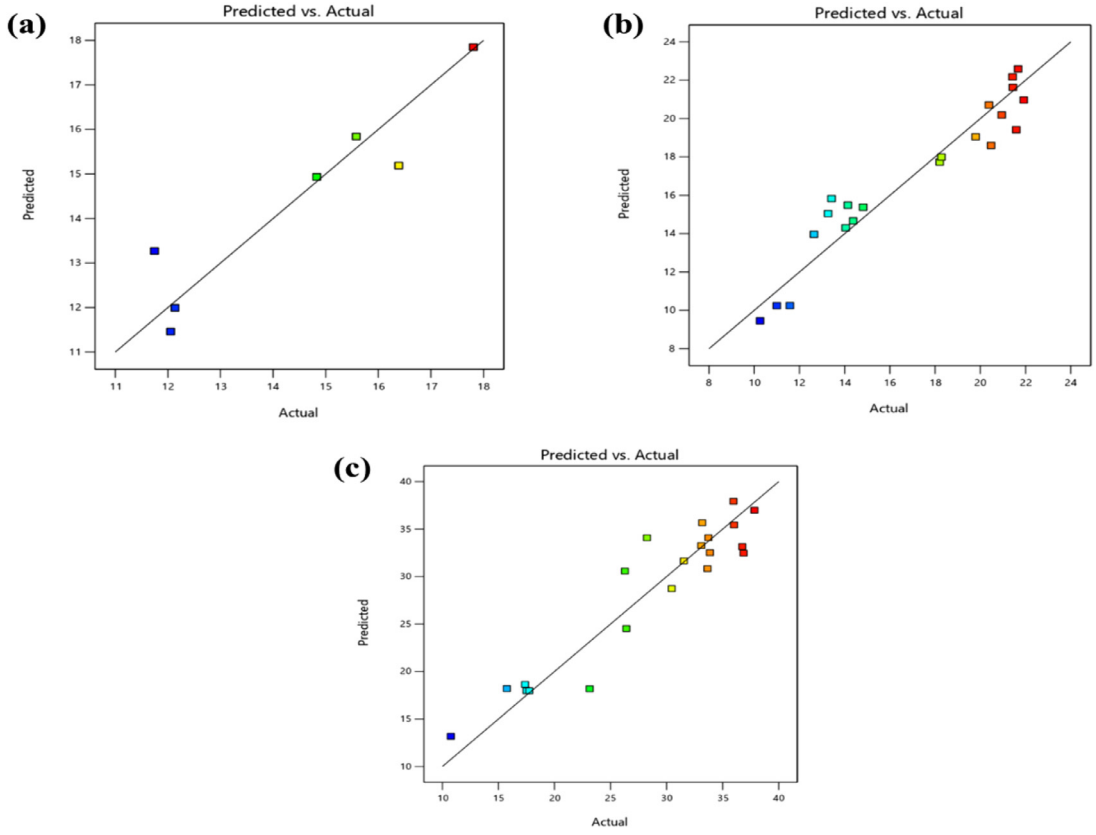

Fig. 13. Diagnostic plots of predicted versus actual values of PVT/PCM system for, (a) Electrical efficiency, (b) Thermal efficiency, (c) Overall efficiency.

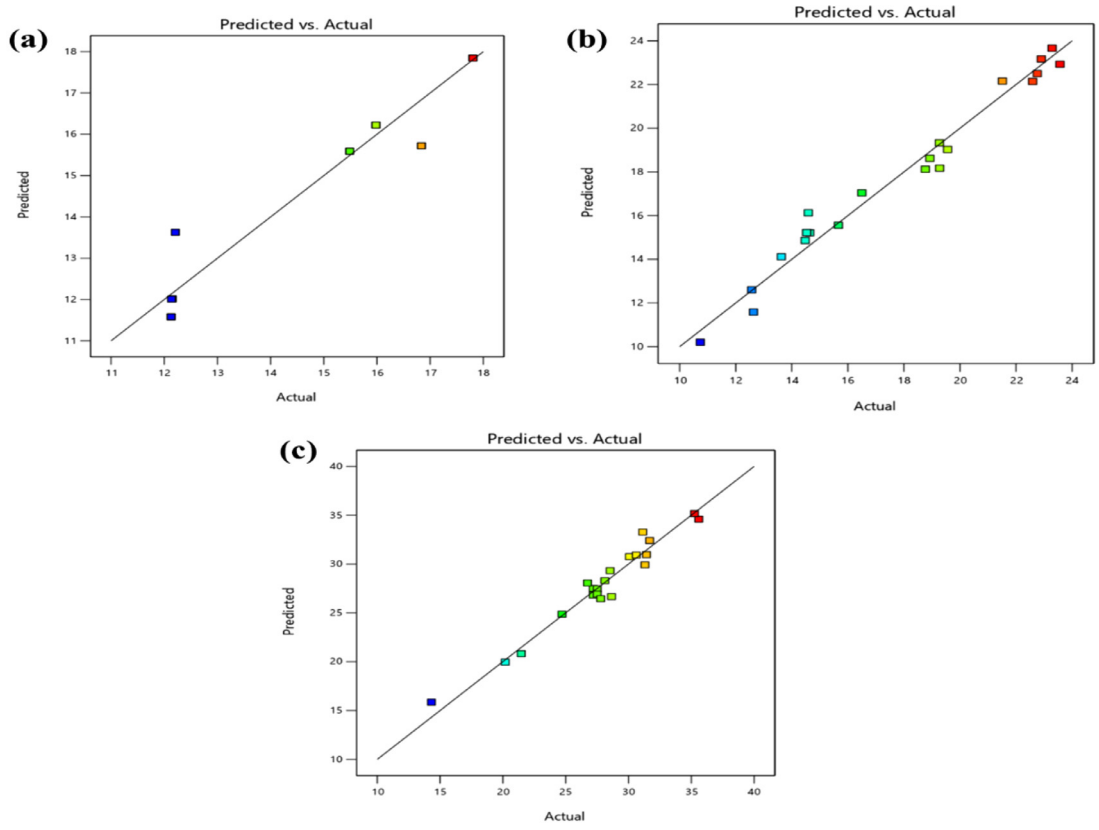

Fig. 14. Diagnostic plots of predicted versus actual values of PVT/HNPCM system for, (a) Electrical efficiency, (b) Thermal efficiency, (c) Overall efficiency.

Table 15
Optimum values for PVT/PCM system for each goal using single-objective optimization.

Goals of optimization	Optimum operating factors				
	Daytime (AM/PM)	Intensity (W/m^2)	Mass flow rate (kg/s)	Predicted response	Desirability
To maximize only electrical efficiency	12.00	750.81	0.002	15.65	0.99
To maximize only thermal efficiency	13.00	789.61	0.002	46.30	0.99
To maximize only overall efficiency	13.00	792.05	0.002	62.38	1.00

Table 16
Optimum values for PVT/HNPCM system for each goal using single-objective optimization.

Goals of optimization	Optimum operating factors				
	Daytime (AM/PM)	Intensity (W/m^2)	Mass flow rate (kg/s)	Predicted response	Desirability
To maximize only electrical efficiency	13.00	735.22	0.002	15.75	0.99
To maximize only thermal efficiency	13.00	781.36	0.002	50.60	0.99
To maximize only overall efficiency	13.00	786.09	0.002	66.99	1.00

Table 17
Optimum values for PVT/PCM system for each goal using multi-objective optimization.

Goals of optimization	Optimum operating factors			Predicted response			Desirability
	Daytime (AM/PM)	Intensity (W/m^2)	Mass flow rate (kg/s)	η_{el}	η_{th}	η_{ov}	
To maximize electrical and thermal efficiency	13.00	798.04	0.002	15.38	46.20	61.58	0.99
To maximize thermal and overall efficiency	13.00	802.27	0.002	15.38	48.35	63.73	1.00
To maximize electrical and overall efficiency	13.00	774.34	0.002	15.48	47.00	62.48	1.00
To maximize electrical, thermal, and overall efficiency	13.00	809.46	0.002	15.68	49.26	63.94	1.00

Table 18
Optimum values for PVT/HNPCM system for each goal using multi-objective optimization.

Goals of optimization	Optimum operating factors			Predicted response			Desirability
	Daytime (AM/PM)	Intensity (W/m^2)	Mass flow rate (kg/s)	η_{el}	η_{th}	η_{ov}	
To maximize electrical and thermal efficiency	13.00	767.97	0.002	15.71	50.60	66.31	0.99
To maximize thermal and overall efficiency	13.00	803.00	0.002	15.71	52.46	67.17	1.00
To maximize electrical and overall efficiency	12.00	757.05	0.002	16.00	51.28	67.42	1.00
To maximize electrical, thermal, and overall efficiency	13.00	774.61	0.002	15.80	52.13	67.13	1.00

mum values of operating factors and optimum values of operating factors for each goal using multi-objective optimization for both PVT/PCM and PVT/HNPCM systems are summarized in Tables 17 and 18. The values of desirability have been found close to the unity which indicates that predicted responses are in the acceptable range.

4.7. Performance assessment of PVT/HNPCM system

4.7.1. Variation of cell temperature

The primary goal of employing PVT/HNPCM and PVT/PCM systems, as previously noted, is to increase the performance of the traditional PV module by cooling the solar cells. As a result, the temperature of the solar cells plays a significant role in photovoltaic systems. Fig. 15. in the study illustrates how using Al_2O_3 and ZnO with the PCM affects the PVT system's surface temperature. As seen at the highest solar irradiation of 870 W/m^2, the maximum cell temperatures of the PVT/HNPCM, PVT/PCM, and PV systems were 56.75 °C, 60.35 °C, and 62.15 °C, respectively. As a result, the average surface temperature was reduced by 5.4 °C when Al_2O_3 and ZnO were combined with the PCM of the PVT system. Furthermore, there was a 3.6 °C difference in the surface temperatures of the PVT/HNPCM and PVT/PCM systems.

4.7.2. Electrical efficiency

The fluctuation of the output electrical powers and electrical efficiencies of the PVT/PCM and PVT/HNPCM systems are shown in Figs. 16 and 17, respectively. From Fig. 16, it is obvious that the PVT/PCM system's output electrical powers were increased close to solar noon. This occurs as a result of the system's increased absorption of solar light. Additionally, the PVT/HNPCM system, PVT/PCM system, and PV system have maximum electrical output powers of 16.18 W, 15.85 W, and 12.32 W, respectively. Thus, the maximum output electrical power is increased by nearly 3.86 W (i.e., around 31.33 %) when the photovoltaic thermal system and hybrid nanomaterials were used in conjunction with the PCM than PV panel because of a lower cell temperature of the PVT/HNPCM system. The maximum electrical energy efficiencies of the PVT/HNPCM system, PVT/PCM and the PV system are 15.71 %, 15.38 % and 11.95 %, respectively. As a result, the PVT/HNPCM system's electrical energy efficiency has been increased by approximately 31.46 % when compared to a conventional PV module. It is evident that the maximum electrical power and efficiency takes place at the peak hours of the day. The results also elucidate better performances for PVT/HNPCM than PVT/PCM for both the parameters. Additionally, it has been found that the electrical power and efficiency of PVT/HNPCM are approximately 2.08 % and 2.15 %, respectively higher than PVT/PCM.

4.7.3. Thermal efficiency

The variations of thermal power and thermal efficiency of the PVT/PCM and PVT/HNPCM throughout the day at uniform mass flow of 0.0021 kg/s (due to the elevation of overhead tank from the floor), as depicted in Figs. 18 and 19. It has been found that PVT/HNPCM has a greater thermal efficiency than PVT/PCM due to the hybrid nano-PCM having improved thermal conductivity, which enables a faster rate of

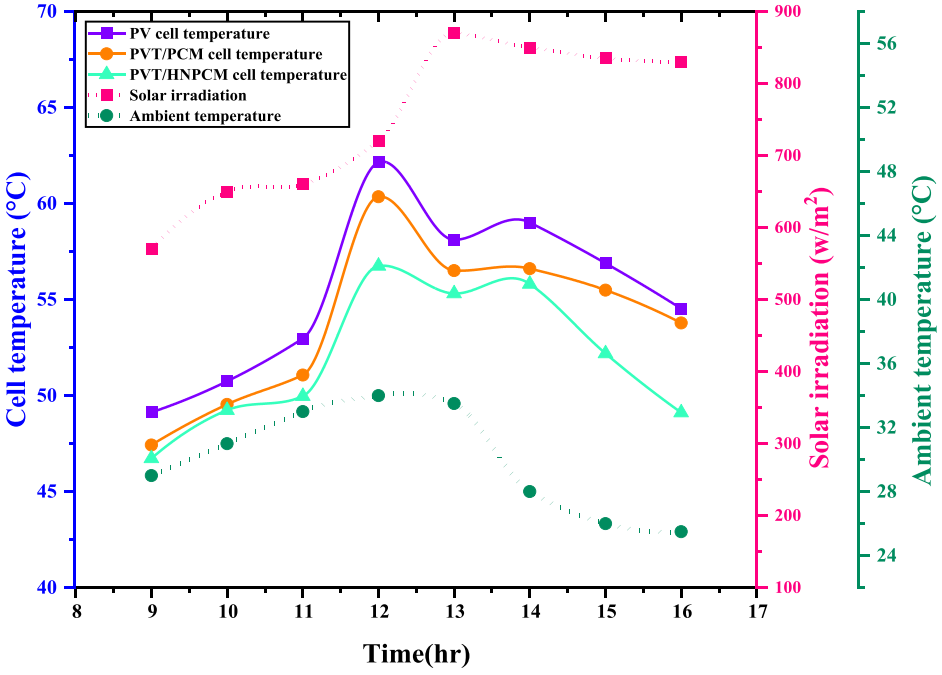

Fig. 15. Variations of the cells temperature and solar irradiance for the conventional PV module, the PVT/PCM and PVT/HNPCM systems.

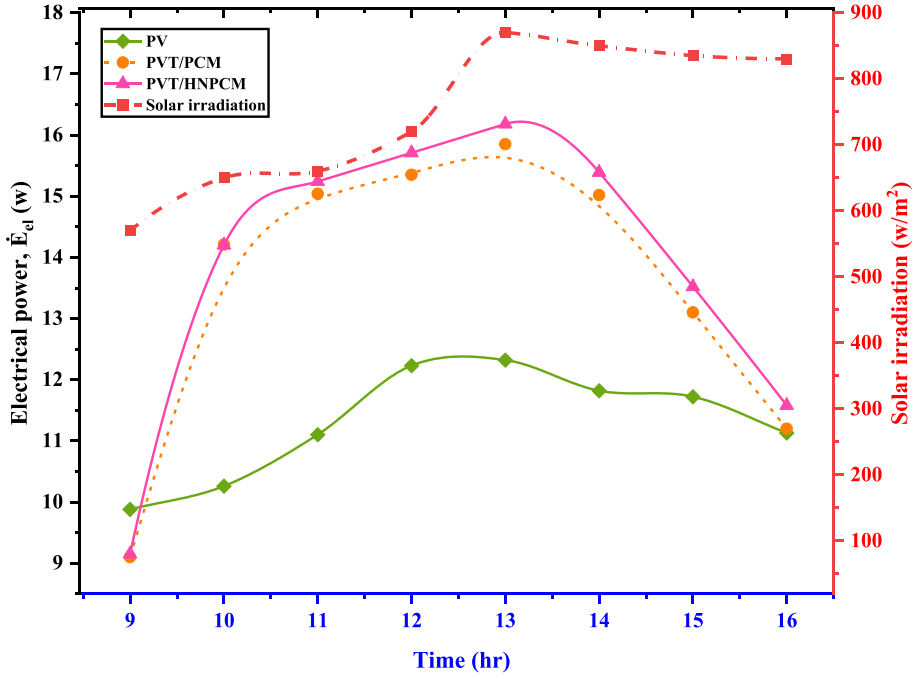

Fig. 16. Variations of output electrical power of PV, PVT/PCM, PVT/HNPCM systems.

heat transfer to water. Thus, the maximum output thermal power in comparison with PVT/PCM system is increased by nearly 5.83 W (i.e., around 12.4 %) when the photovoltaic thermal system and hybrid nano-materials were used in conjunction with the PCM. Thermal efficiency is 47 % with PVT/PCM and 51.28 % with PVT/HNPCM system at the mass flow rate of 0.0021 kg/s. It is apparently seen from the Fig. 18 that there is a gradual declination in thermal power and efficiency due to declining the cell temperature of the panel, the intensity of the solar radiation, and the heat storing capacity of the PCM and HNPCM. The results of this investigation show that the PVT with hybrid nano-particle integrated PCM outperforms the PVT with only PCM in terms of thermal power and efficiency.

4.7.4. Overall efficiency

The PVT/PCM and PVT/HNPCM system's overall efficiency for the optimum flowrate at 0.0021 kg/s throughout the day from 9AM to 4PM has been exhibited in Fig. 20. The addition of hybrid nanoparticles in PCM is shown to have higher overall efficiency than PVT/PCM for any abscissa due to having higher thermal conductivity and heat extraction rate from the panel for PVT/HNPCM system. The overall efficiency in both situations was steadily increased in the morning before declining around noon as a result of decreasing solar irradiation. Due to that day's peak solar radiation, the maximum overall efficiency was figured out to be around 66.31 % for PVT/HNPCM and 61.58 % for PVT/PCM. Additionally, it is speculated that the PVT/HNPCM

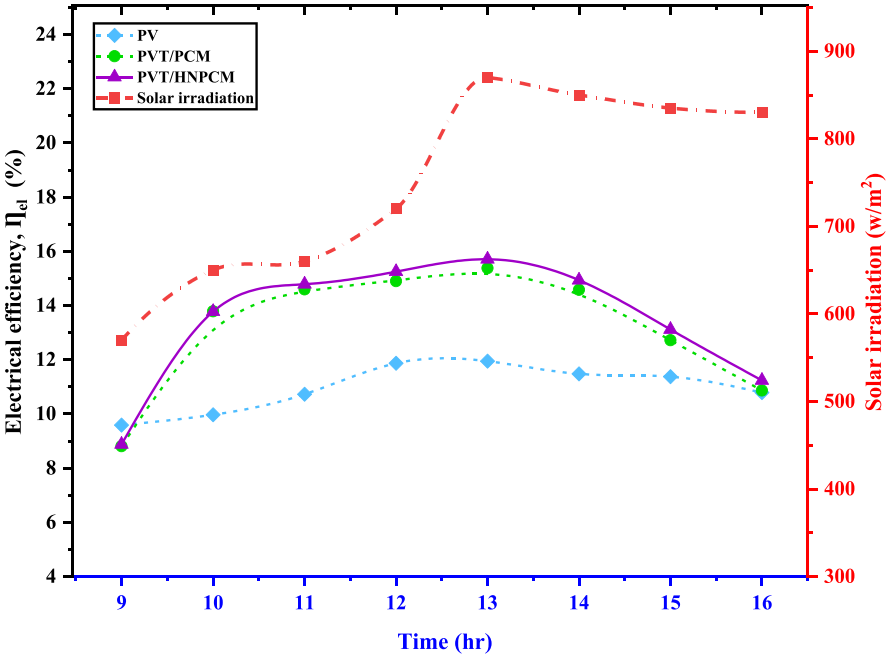

Fig. 17. Variations of output electrical efficiency of PV, PVT/PCM, PVT/HNPCM systems.

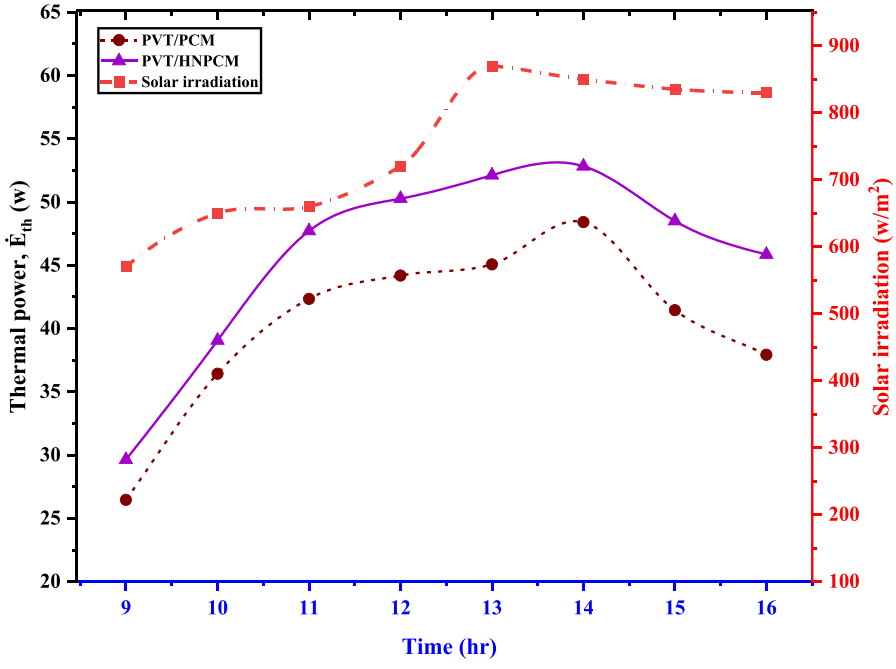

Fig. 18. Variations of output thermal power of PV, PVT/PCM, PVT/HNPCM systems.

system has an overall efficiency difference that was approximately 7.68 % higher than the PVT/PCM system. It is clearly evident from Fig. 20 that the PVT/HNPCM system performs better than the PVT/PCM system.

4.8. RSM model verification

The maximum experimental findings are validated with the obtained maximum values of electrical, thermal, and overall efficiency simultaneously at the optimum condition of operating factors by analysis the RSM and the error rates are investigated. Two random experiments were carried out based on the planning obtained by the RSM method and the maximum experimental outcomes are compared with the optimum values of responses obtained from the mathematical model generated by the RSM method for both the PVT/PCM and PVT/HNPCM systems. The verification results of the mathematical models with the error from the maximum experimental outcomes are tabulated in Table 19 for both systems (PVT/PCM and PVT/HNPCM). After the verification, the error rate is figured out, and it is seen that the error rate is in the acceptable range [70,71]. After completing the comparisons from experimental outcomes, the error rate for electrical, thermal, and overall efficiency is estimated by around −1.95 % and −0.57 %, −4.81 % and −1.66 %, and −3.83 % and −1.24 % respectively for both the PVT/PCM and PVT/HNPCM systems.

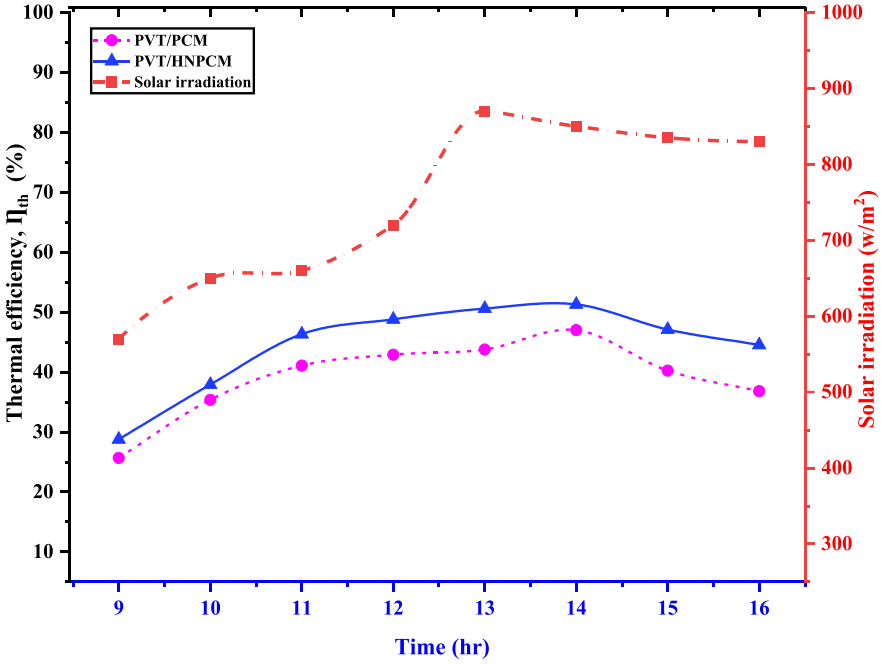

Fig. 19. Variations of output thermal efficiency of PV, PVT/PCM, PVT/HNPCM systems.

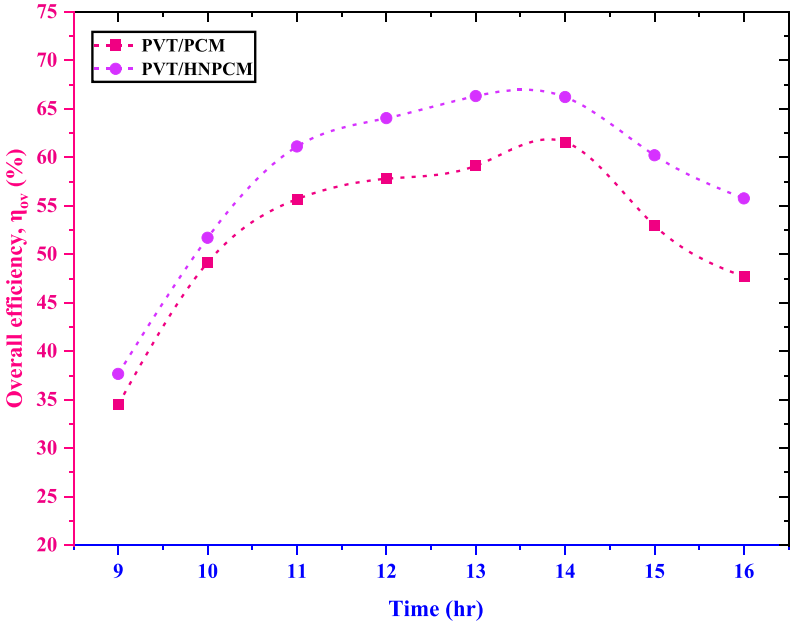

Fig. 20. Overall efficiency of PVT/PCM and PVT/HNPCM.

Table 19
Verification results of the mathematical models for PVT/PCM and PVT/HNPCM systems.

Systems	Optimum Operating factors			Electrical Efficiency			Thermal Efficiency			Overall Efficiency		
	Daytime (AM/PM)	Intensity (W/m^2)	Mass flow rate (kg/s)	Experimental	Model	Error (%)	Experimental	Model	Error (%)	Experimental	Model	Error (%)
PVT/PCM	13.00	809.46	0.002	15.38	15.68	−1.95	47	49.26	−4.81	61.58	63.94	−3.83
PVT/HNPCM	13.00	774.61	0.002	15.71	15.80	−0.57	51.28	52.13	−1.66	66.31	67.13	−1.24

4.9. Comparison with literature

Comparing the three experimental setups reveals that PVT/HNPCM (2 % Al_2O_3 and ZnO nanoparticles with PCM) performs better than PVT/PCM and conventional PV panel setups. To put things in perspective, the most compelling findings from this study have been contrasted with those from earlier research that can be found in the literature. This comparison was based on modification similarities and corresponding percentage improvements, which supports the merit of the configuration suggested in the current study as shown in Table 20.

Table 20
Comparison of the present work with the previously conducted similar studies.

References	Country	Configurations	Improved efficiency	
			Electrical	Thermal
[45]	Malaysia	PV/T with SiC-nano fluid and SiC-nano PCM with mass flow rate of working fluid ranging from 0.008 kg/s to 0.058 kg/s.	9.6 %	77.5 %
[34]	India	Paraffin wax RT-30 in water-based PV/T-PCM.	11.32 %	33.81–62.37 %
[42]	Saudi Arabia	PVT/nano PCM with Eutectic of capric and palmitic acid, $CaCl_2{\cdot}6H_2O$, Paraffin wax as PCM with GnP nanoparticles	6.9–22 %	–
[40]	Egypt	PV/T-nano PCM $CaCl_2{\cdot}6H_2O$ as PCM+Al_2O_3 nanoparticles and compound cooling.	13 %	68.4 %
[72]	Ghana	A water-based flat plate PVT was investigated under the mass flow rate from 0.025 kg/s to 0.083 kg/s.	10.12–10.83 %	42.46–45.60 %
Present work	Bangladesh	PVT system, passive cooling with paraffin wax (PCM) incorporating hybrid nanoparticles (Al_2O_3 and ZnO) 2 wt%.	15.71 %	51.28 %

[a]Compared to the relevant baseline (conventional) scenario.

5. Conclusions and future recommendations

In this study, PVT systems were developed to integrate solar PV and thermal collectors to generate electricity and heat energy simultaneously. The primary objective was to examine how the performance of PVT systems was affected by the use of hybrid nano PCM (HNPCM, PCM combined with Al_2O_3 and ZnO) at different compositions of 0.5 %, 1 %, and 2 %. A comparative performance analysis of conventional PVT, PVT/PCM, and the PVT/HNPCM was carried out. The followings can be concluded from the investigation:

- The FTIR test was conducted to determine the chemical bond in the samples and the outcome suggest that the addition of hybrid nanoparticles into paraffin wax has not changed the original outcome of pure paraffin wax due to no existence of new chemical bonds and indicates the uniform distribution of nano-particles into paraffin wax.
- Scanning electron microscope (SEM) test was conducted for the morphological analysis of the samples and the test results show that 2 % of hybrid nanoparticles mixed with PCM exhibited better connection with base paraffin wax without having any agglomeration.
- A TGA test was performed to distinguish the thermal stability property among the samples and the test elucidates better thermal stability for 2 % mass of hybrid nanoparticles than others. 2 % mass of hybrid nanoparticles were found to have around 11 % residual mass at 500 ˚C temperature.
- Thermal conductivity test was performed for the samples by thermal conductivity tester DTC-25. 2 % of hybrid nano-PCM shows higher thermal conductivity of 2.18 W/mK than pure paraffin wax (1.54 W/mK). The outcome shows the gradual increment of thermal conductivity by the addition of hybrid nanoparticles having mass fractions 0.5, 1, and 2 % respectively. The percentage increment of thermal conductivity was found by about 24.68 %, 28.57 %, and 41.56 % for the sample having mass fractions 0.5 %, 1 %, and 2 % respectively.
- Differential scanning calorimetry (DSC) test was performed to determine the melting point temperature and latent heat of capacity for every sample. The melting point temperature was found to be by about 61.56 ˚C, 60.88 ˚C, 60.52 ˚C, and 60.07 ˚C for the samples having a mass fraction of hybrid nano-particles 0 %, 0.5 %, 1 %, and 2 % respectively. The latent heat capacity was found to be about 234.52 kJ/kg, 232.13 kJ/kg, 230.32 kJ/kg, and 228.93 kJ/kg for the samples having mass fractions of hybrid nano-particles 0 %, 0.5 %, 1 %, and 2 %, respectively.
- The single-objective optimization demonstrates that the maximum predicted values of electrical, thermal, and overall efficiency are 15.65 % and 15.75 %, 46.30 % and 50.60 %, and 62.38 % and 66.99 % respectively for PVT/PCM and PVT/HNPCM systems.
- For the objective of optimizing electrical, thermal, and overall efficiency simultenously, the maximum predicted electrical, thermal, and overall efficiency are 15.68 % and 15.80 %, 49.26 % and 52.13 %, and 63.94 % and 67.13 % respectively for PVT/PCM and PVT./HNPCM systems and the values of desirability for single and multi-objective optimization are close to unity which refers that the predicted responses for all goals are in the acceptable range.
- The predicted model suggests that the highest electrical, thermal, and overall efficiency, simultaneously, can be obtained by using following conditions: the identical daytime of 13.00PM, solar intensity of 809 W/m^2 and 774 W/m^2, and identical mass flow rate of 0.002 kg/s for both the PVT/PCM and PVT/HNPCM systems.
- The maximum PV cell temperatures were obtained as 62.15 ˚C, 60.35 ˚C, and 56.75 ˚C for only PV, PVT/PCM, and PVT/HNPCM, respectively.
- The maximum electrical efficiencies were achieved as 11.95 %, 15.38 %, and 15.71 % for the PV, PVT/PCM, and PVT/HNPCM systems, respectively, which were enhanced by 28.70 % and 31.46 % respectively than the conventional PV panel.
- The highest thermal efficiency was achieved at 47 % and 51.28 % respectively for PVT/PCM and PVT/HNPCM systems at the mass flow rate 0.0021 kg/s.
- The overall efficiency was obtained at around 61.58 % and 66.31 % respectively for PVT/PCM and PVT/HNPCM systems.
- Additionally, each response's diagnostic analysis was completed to demonstrate the predictive model's respectable accuracy. The statistical significance and suitability of the RSM model was further assessed using the ANOVA test.

In this study, authors have investigated the performance of PV panels at a lower range of mass flow rate of working fluid (water). However, the thermal efficiency is the function of the mass flow rate and a lower mass flow rate restricts the thermal efficiency. The usage of higher and varying mass flow rates on the performance of PV panels along with the economical evaluation can be deemed as further research investigation to compensate the lowest values of thermal efficiency for both the systems. Additionally, it is possible to carry out the further study employing hybrid nano-particles in water to form nanofluid instead of using only water as working fluid. Moreover, authors believe that implementation of nanofluid along with the inclusion of extended surface (fins) can improve the system performance. The impacts of inclusion nano-enhanced PCM or nanofluid for the environment and ecosystem when it leaks or spills out from the system should be considered for the further investigation because their environmental effects are not thoroughly blessings. Additionally, the numerical investigation using the computational fluid dynamics (CFD) can be employed to validate the experimental result. Finally, it is required to investigate the seasonal variations on the perfor-

mance of photovoltaic panel by the inclusion of hybrid nano-enhanced PCM.

Funding declaration

Authors have not received any funding to carry out the project.

Declaration of competing interest

The authors declare that they have no known competing financial interests or personal relationships that could have appeared to influence the work reported in this paper.

CRediT authorship contribution statement

Md. Golam Kibria: Conceptualization, Methodology, Investigation, Writing – original draft, Writing – review & editing. **Utpol K. Paul:** Software, Methodology, Investigation, Writing – original draft, Writing – review & editing. **Md. Shahriar Mohtasim:** Methodology, Formal analysis, Visualization, Writing – review & editing. **Barun K. Das:** Supervision, Writing – review & editing. **N.N. Mustafi:** Writing – review & editing.

Acknowledgment

The support from Department of Mechanical Engineering, Rajshahi University of Engineering & Technology (RUET) is highly appreciated.

References

[1] X. Wen, et al., Performance assessment of the hybrid PV-MCHP-TE system integrated with PCM in all-day operation: a preliminary numerical investigation, Energy 278 (2023) 127932.
[2] R.A. Mangkuto, D.N.A.T. Tresna, I.M. Hermawan, J. Pradipta, N. Jamala, B. Paramita, Atthaillah, Experiment and simulation to determine the optimum orientation of building-integrated photovoltaic on tropical building façades considering annual daylight performance and energy yield, Energy Built Environ (2024) 414–425.
[3] M.G. Kibria, U.K. Paul, A. Hasan, M.S. Mohtasim, B.K. Das, M. Mourshed, Current prospects and challenges for biomass energy conversion in Bangladesh: attaining sustainable development goals, Biomass and Bioenergy 183 (2024) 107139.
[4] M.M. Ahmed, B.K. Das, P. Das, M.S. Hossain, M.G. Kibria, Energy management and sizing of a stand-alone hybrid renewable energy system for community electricity, fresh water, and cooking gas demands of a remote island, Energy Convers. Manag. 299 (2024) 117865.
[5] U.A. Anika, Md.G. Kibria, S.D. Kanka, Md.S. Mohtasim, U.K. Paul, B.K. Das, Exergy, exergo-economic, environmental and sustainability analysis of pyramid solar still integrated hybrid nano-PCM, black sand, and sponge, Sol. Energy 274 (2024) 112559.
[6] P. Wei, et al., Bibliographical progress in hybrid renewable energy systems' integration, modelling, optimization, and artificial intelligence applications: a critical review and future research perspective, Energy Sources A: recovery Util, Environ. Eff. 45 (2023) 2058–2088.
[7] Md.S. Mohtasim, B.K. Das, Biomimetic and bio-derived composite Phase Change Materials for Thermal Energy Storage applications: a thorough analysis and future research directions, J. Energy Storage 84 (2024) 110945.
[8] A. Alexander Stonier, et al., An extensive critique on fault-tolerant systems and diagnostic techniques intended for solar photovoltaic power generation, Energy Sources A: recovery Util, Environ. Eff. 45 (2023) 1856–1873.
[9] Y. Hu, Q. Xue, H. Wang, P. Zou, J. Yang, S. Chen, Y. Cheng, Experimental investigation on indoor daylight environment of building with Cadmium Telluride photovoltaic window, Energy Built Environ. 5 (2024) 404–413.
[10] N. Farouk, et al., Thermal performance analysis of artificially roughened solar air heater under turbulent pulsating flow with various wave shapes, Case Stud. Ther. Eng. 41 (2023) 102664.
[11] S. Kumari, et al., Efficiency enhancement of photovoltaic panel by heat harvesting techniques, Energy Sustain. Dev. 73 (2023) 303–314.
[12] P.K.S. Rathore, et al., Beeswax as a potential replacement of paraffin wax as shape stabilized solar thermal energy storage material: an experimental study, J. Energy Storage 68 (2023) 107714.
[13] M.G. Kibria, M.S. Mohtasim, U.K. Paul, B.K. Das, R. Saidur, Impact of hybrid nano PCM (paraffin wax with Al2O3 and ZnO nanoparticles) on photovoltaic thermal system: energy, exergy, exergoeconomic and enviroeconomic analysis, J. Clean. Prod. 436 (2024) 140577.
[14] R.M. Elavarasan, et al., Pathways toward high-efficiency solar photovoltaic thermal management for electrical, thermal and combined generation applications: a critical review, Energy Convers. Manag. 255 (2022) 115278.
[15] D. Govindasamy, A. Kumar, Evaluation of the impact of different composite phase change materials on reduction in temperature and enhancement of solar panel efficiency, J. Energy Storage 60 (2023) 106631.
[16] M.S. Ahmed, R. Karal, B.K. Das, A. Das, Experimental investigation of cooling, wind velocity, and dust deposition effects on solar PV performance in a tropical climate in Bangladesh, Case Stud. Therm. Eng. 50 (2023) 103409.
[17] A. Hassan, et al., An experimental and numerical study on the impact of various parameters in improving the heat transfer performance characteristics of a water based photovoltaic thermal system, Renew. Energy 202 (2023) 499–512.
[18] PV module technical data sheet. Available online: https://us.sunpower.com/sites/default/files/sunpower-e-series-commercial-solar-panels-e20-327-com-datasheet-505701-revh.pdf (accessed on 05 January 2023).
[19] S.R. Madas, R. Narayanan, P. Gudimetla, Numerical investigation on the optimum performance output of photovoltaic thermal (PVT) systems using nano-copper oxide (CuO) coolant, Sol. Energy 255 (2023) 222–235.
[20] M. Ahmadinejad, R. Moosavi, Energy and exergy evaluation of a baffled-nanofluid-based photovoltaic thermal system (PVT), Int. J. Heat Mass Transf. 203 (2023) 123775.
[21] A. Maleki, et al., A review on the approaches employed for cooling PV cells, Sol. Energy 209 (2020) 170–185.
[22] L.A. Ahmadlou, et al., Experimental investigation of PV/T and thermoelectric systems using CNT/water nanofluids, Appl. Therm. Eng. 227 (2023) 120350.
[23] G. Asefi, T. Ma, R. Wang, Techno-economic evaluation of photovoltaic thermal system integrated with porous phase change materials: case studies in China, Energy Convers. Manag. 290 (2023) 117227.
[24] S.K. Pathak, et al., A detailed review on the performance of photovoltaic/thermal system using various cooling methods, Sustain. Energy Technol. Assess. 51 (2022) 101844.
[25] F. Jamil, et al., Thermal regulation of photovoltaics using various nano-enhanced phase change materials: an experimental study, J. Clean. Prod. 414 (2023) 137663.
[26] M. Moein-Jahromi, et al., Evaluation of nanostructured GNP and CuO compositions in PCM-based heat sinks for photovoltaic systems, J. Energy Storage 53 (2022) 105240.
[27] A. Karaipekli, et al., Thermal characteristics of expanded perlite/paraffin composite phase change material with enhanced thermal conductivity using carbon nanotubes, Energy convers. manag. 134 (2017) 373–381.
[28] S.D. Kanka, et al., Impact of various environmental parameters and production enhancement techniques on direct solar still: a review, Sol. Energy 267 (2024) 112216.
[29] R. Sharma, P. Ganesan, V. Tyagi, Long-term thermal and chemical reliability study of different organic phase change materials for thermal energy storage applications, J. Therm. Anal. Calorim. 124 (2016) 1357–1366.
[30] T. Wongwuttanasatian, T. Sarikarin, A. Suksri, Performance enhancement of a photovoltaic module by passive cooling using phase change material in a finned container heat sink, Sol. Energy 195 (2020) 47–53.
[31] H. Gürbüz, et al., Experimental investigation on electrical power and thermal energy storage performance of a solar hybrid PV/T-PCM energy conversion system, J. Build. Eng. 69 (2023) 106271.
[32] M. Hossain, et al., Two side serpentine flow based photovoltaic-thermal-phase change materials (PVT-PCM) system: energy, exergy and economic analysis, Renew. Energy 136 (2019) 1320–1336.
[33] M. Rezvanpour, et al., Using CaCl2· 6H2O as a phase change material for thermo-regulation and enhancing photovoltaic panels' conversion efficiency: experimental study and TRNSYS validation, Renew. Energy 146 (2020) 1907–1921.
[34] S. Preet, B. Bhushan, T. Mahajan, Experimental investigation of water based photovoltaic/thermal (PV/T) system with and without phase change material (PCM), Sol. Energy 155 (2017) 1104–1120.
[35] J. Paul, et al., A comprehensive review on thermophysical properties and solar thermal applications of organic nano composite phase change materials, J. Energy Storage 45 (2022) 103415.
[36] G.K. Amudhalapalli, J.K. Devanuri, Synthesis, characterization, thermophysical properties, stability and applications of nanoparticle enhanced phase change materials–A comprehensive review, Therm.Sci. Eng. Prog. 28 (2022) 101049.
[37] P.M. Kumar, et al., Investigating thermal properties of Nanoparticle Dispersed Paraffin (NDP) as phase change material for thermal energy storage, Mater. Today: Proc. 45 (2021) 745–750.
[38] K.Y. Leong, M.R.A. Rahman, B.A. Gurunathan, Nano-enhanced phase change materials: a review of thermo-physical properties, applications and challenges, J. Energy Storage 21 (2019) 18–31.
[39] A.N. Keshteli, M. Sheikholeslami, Nanoparticle enhanced PCM applications for intensification of thermal performance in building: a review, J. Mol. Liq. 274 (2019) 516–533.
[40] M. Salem, et al., Performance enhancement of the photovoltaic cells using Al2O3/PCM mixture and/or water cooling-techniques, Renew. Energy 138 (2019) 876–890.
[41] A.H. Al-Waeli, et al., Experimental investigation of using nano-PCM/nanofluid on a photovoltaic thermal system (PVT): technical and economic study, Therm. Sci. Eng. Prog. 11 (2019) 213–230.
[42] A. Abdelrazik, F. Al-Sulaiman, R. Saidur, Numerical investigation of the effects of the nano-enhanced phase change materials on the thermal and electrical performance of hybrid PV/thermal systems, Energy Convers. Manag. 205 (2020) 112449.
[43] M. Islam, et al., Real time experimental performance investigation of a NePCM based photovoltaic thermal system: an energetic and exergetic approach, Renew. Energy 172 (2021) 71–87.
[44] L. Liu, J. Niu, J.-Y. Wu, Improving energy efficiency of photovoltaic/thermal systems by cooling with PCM nano-emulsions: an indoor experimental study, Renew. Energy 203 (2023) 568–582.

[45] A.M. Bassam, et al., Experimental analysis for the photovoltaic thermal collector (PVT) with nano PCM and micro-fins tube nanofluid, Case Stud, Therm. Eng. 41 (2023) 102579.
[46] M. Sharaf, A. Huzayyin, M.S. Yousef, Performance enhancement of photovoltaic cells using phase change material (PCM) in winter, Alex. Eng. J. 61 (2022) 4229–4239.
[47] M.A. Sheik, et al., Investigation on the thermal management of solar photo voltaic cells cooled by phase change material, J. Energy Storage 52 (2022) 104914.
[48] R. Gad, et al., Evaluation of thermal management of photovoltaic solar cell via hybrid cooling system of phase change material inclusion hybrid nanoparticles coupled with flat heat pipe, J. Energy Storage 57 (2023) 106185.
[49] S. Preet, S. Mathur, J. Mathur, M.K. Sharma, A. Chowdhury, Energy characterization of forced ventilated Photovoltaic-DSF system in hot summer of composite climate, Energy Built Environ. 5 (2024) 704–718.
[50] M. Shirinbakhsh, L.D.D. Harvey, Feasibility of achieving net-zero energy performance in high-rise buildings using solar energy, Energy Built Environ. 5 (2024) 946–956.
[51] A. Miglioli, N. Aste, C. Del Pero, F. Leonforte, Photovoltaic-thermal solar-assisted heat pump systems for building applications: integration and design methods, Energy Built Environ. 4 (2023) 39–56.
[52] G. Aspetakis, Q. Wang, Critical review of Air-Based PVT technology and its integration to building energy systems, Energy Built Environ (2023).
[53] X. Zhu, X. Zhang, P. Gong, Y. Li, A review of distributed energy system optimization for building decarbonization, J. Build. Eng. 73 (2023) 106735.
[54] F. Jamil, et al., Evaluation of photovoltaic panels using different nano phase change material and a concise comparison: an experimental study, Renew. Energy 169 (2021) 1265–1279.
[55] F. Schiro, et al., Improving photovoltaics efficiency by water cooling: modelling and experimental approach, Energy 137 (2017) 798–810.
[56] H. Bahaidarah, et al., Performance evaluation of a PV (photovoltaic) module by back surface water cooling for hot climatic conditions, Energy 59 (2013) 445–453.
[57] H. Fayaz, et al., Numerical and outdoor real time experimental investigation of performance of PCM based PVT system, Sol. Energy 179 (2019) 135–150.
[58] J.M. Abdollahzadeh, J.H. Park, Effects of Brownian motion on freezing of PCM containing nanoparticles, Therm. Sci. 20 (2016) 1533–1541.
[59] B. Li, et al., Optimized energy distribution management in the nanofluid-assisted photovoltaic/thermal system via exergy efficiency analysis, Energy 242 (2022) 123018.
[60] F. Yazdanifard, M. Ameri, R.A. Taylor, Numerical modeling of a concentrated photovoltaic/thermal system which utilizes a PCM and nanofluid spectral splitting, Energy Convers. Manag. 215 (2020) 112927.
[61] S. Manigandan, V. Kumar, Comparative study to use nanofluid ZnO and CuO with phase change material in photovoltaic thermal system, Int. J. Energy Res. 43 (2019) 1882–1891.
[62] B. Tang, M. Qiu, S. Zhang, Thermal conductivity enhancement of PEG/SiO2 composite PCM by in situ Cu doping, Sol. Energy Mater. Sol. Cells 105 (2012) 242–248.
[63] R. Gao, et al., like graphene-Ag composite films with enhanced mechanical and electrical properties, Nanoscale res. lett. 8 (2013) 1–8.
[64] J. Shen, et al., One-pot hydrothermal synthesis of Ag-reduced graphene oxide composite with ionic liquid, J. Mater. Chem. 21 (2011) 7795–7801.
[65] S.C. Lin, H.H. Al-Kayiem, Evaluation of copper nanoparticles–Paraffin wax compositions for solar thermal energy storage, Sol. Energy 132 (2016) 267–278.
[66] J. Zhou, M. Hatami, D. Song, D. Jing, Design of microchannel heat sink with wavy channel and its time-efficient optimization with combined RSM and FVM methods, Int. J. Heat Mass Transf. 103 (2016) 715–724.
[67] M. Rahimi-Gorji, O. Pourmehran, M. Hatami, D.D. Ganji, Statistical optimization of microchannel heat sink (MCHS) geometry cooled by different nanofluids using RSM analysis, Eur. Phys. J. Plus 130 (2015) 15022–15028.
[68] R.k. Bett, A. Kumar, Z.O. Siagi, Optimization of liquid fuel production from microwave pyrolysis of used tyres, J. Energy (2021) 1–11.
[69] R. Idris, C.T. Chong, J.A. Asik, F.N. Ani, Optimization studies of microwave-induced co-pyrolysis of empty fruit bunches/waste truck tire using response surface methodology, J. Clean. Prod. 244 (2020) 118649.
[70] K. Gelis, A.N. Celik, K. Ozbek, O. Ozyurt, Experimental investigation into efficiency of SiO2/water-based nanofluids in photovoltaic thermal systems using response surface methodology, Sol. Energy 235 (2022) 229–241.
[71] O. Rejeb, C. Ghenai, M.H. Jomaa, M. Bettayeb, Statistical study of a solar nanofluid photovoltaic thermal collector performance using response surface methodology, Case Stud. Therm. Eng. 21 (2020) 100721.
[72] S. Abdul-Ganiyu, D.A. Quansah, E.W. Ramde, R. Seidu, M.S. Adaramola, Study effect of flow rate on flat-plate water-based photovoltaic-thermal (PVT) system performance by analytical technique, J. Clean. Prod. 321 (2021) 128985.